



Since January 2020 Elsevier has created a COVID-19 resource centre with free information in English and Mandarin on the novel coronavirus COVID-19. The COVID-19 resource centre is hosted on Elsevier Connect, the company's public news and information website.

Elsevier hereby grants permission to make all its COVID-19-related research that is available on the COVID-19 resource centre - including this research content - immediately available in PubMed Central and other publicly funded repositories, such as the WHO COVID database with rights for unrestricted research re-use and analyses in any form or by any means with acknowledgement of the original source. These permissions are granted for free by Elsevier for as long as the COVID-19 resource centre remains active.



Discovery of novel thioquinazoline-*N*-aryl-acetamide/*N*-arylaceto-hydrazide hybrids as anti-SARS-CoV-2 agents: Synthesis, *in vitro* biological evaluation, and molecular docking studies

Heba T. Abdel-Mohsen^{a,*}, Mohamed A. Omar^a, Omnia Kutkat^b, Ahmed M. El Kerdawy^c, Alaa A. Osman^d, Mohamed GabAllah^b, Ahmed Mostafa^{b,*}, Mohamed A. Ali^b, Hoda I. El Diwani^a

^a Department of Chemistry of Natural and Microbial Products, Pharmaceutical and Drug Industries Research Institute, National Research Centre, El-Buhouth St., Dokki, P.O. Box 12622, Cairo, Egypt

^b Center of Scientific Excellence for Influenza Viruses, National Research Centre, Giza 12622, Egypt

^c Department of Pharmaceutical Chemistry, Faculty of Pharmacy, Cairo University, Kasr El-Aini Street, Cairo, P.O. Box 11562, Egypt

^d Department of Pharmaceutical Chemistry, School of Pharmacy, NewGiza University (NGU), NewGiza, km 22 Cairo–Alexandria Desert Road, Cairo, Egypt

ARTICLE INFO

Article history:

Received 12 August 2022

Revised 10 November 2022

Accepted 29 November 2022

Available online 30 November 2022

Keywords:

Thioquinazoline

SARS-CoV-2

Molecular docking studies

ABSTRACT

In the current investigation, two novel series of (tetrahydro)thioquinazoline-*N*-arylacetamides and (tetrahydro)thioquinazoline-*N*-arylaceto-hydrazides were designed, synthesized and investigated for their antiviral activity against SARS-CoV-2. The thioquinazoline-*N*-arylacetamide **17g** as well as the tetrahydrothioquinazoline-*N*-arylaceto-hydrazides **18c** and **18f** showed potent antiviral activity with IC₅₀ of 21.4, 38.45 and 26.4 μM, respectively. In addition, **18c** and **18f** demonstrated potential selectivity toward the SARS-CoV-2 over the host cells with *SI* of 10.67 and 16.04, respectively. Further evaluation of the mechanism of action of the three derivatives **17g**, **18c**, and **18f** displayed that they can inhibit the virus at the adsorption as well as at the replication stages, in addition to their virucidal properties. In addition, **17g**, **18c**, and **18f** demonstrated satisfactory physicochemical properties as well as drug-likeness properties to be further optimized for the discovery of novel antiviral agents. The docking simulation on M^{PRO} binding site predicted the binding pattern of the target compounds rationalizing their differential activity based on their hydrophobic interaction and fitting in the hydrophobic S2 subsite of the binding site

© 2022 Elsevier B.V. All rights reserved.

1. Introduction

Recently, coronavirus disease 2019 (COVID-19) has been identified as a global pandemic disease that affects the survival of population all over the world [1]. COVID-19 is a respiratory disease that causes upper and lower respiratory tract infection which can be further progressed further into respiratory failure by complex mechanisms and may end up with premature mortality [1,2]. It was reported that COVID-19 is caused by a novel zoonotic member of betacoronaviruses called severe acute respiratory syndrome coronavirus 2 (SARS-CoV-2) which is a single stranded RNA virus of the Coronaviridae family [3,4].

The huge problem, which is currently facing the world, is the remarkable ability of SARS-CoV-2 to mutate over a short period of

time [5]. Hence, a plethora of studies have been performed to get some insightful knowledge about SARS-CoV-2 virus [6]. Successfully, some information has been reported including its molecular structure, life cycle, and its interactions with the host cells. This enabled the development various vaccines with different mechanisms of action to be used by humans [7].

Up till now, the effective and specific antiviral agents for the treatment of SARS-CoV-2 infection are limited or rare [8]. Hence, numerous investigations have been carried out to identify new targets to control this pathogen without affecting the host cells. Recently, some structural elements that can act as potential therapeutic targets have been recognized. Spike glycoprotein was identified as a promising target that is present on the virus surface, and it is responsible for the virus binding to the host cell [9]. RNA-dependent RNA polymerase (RdRp) is another attractive target participating in the replication of RNA from an RNA template [10]. Meanwhile, the 3-C-like protease (3CL^{PRO} or M^{PRO}) and papain-like protease (PL^{PRO}) were pointed out to be the most important targets

* Corresponding authors.

E-mail addresses: ht.abdel-mohsen@nrc.sci.eg, hebadelmohsen@gmail.com (H.T. Abdel-Mohsen), ahmed_elsayed@daad-alumni.de (A. Mostafa).

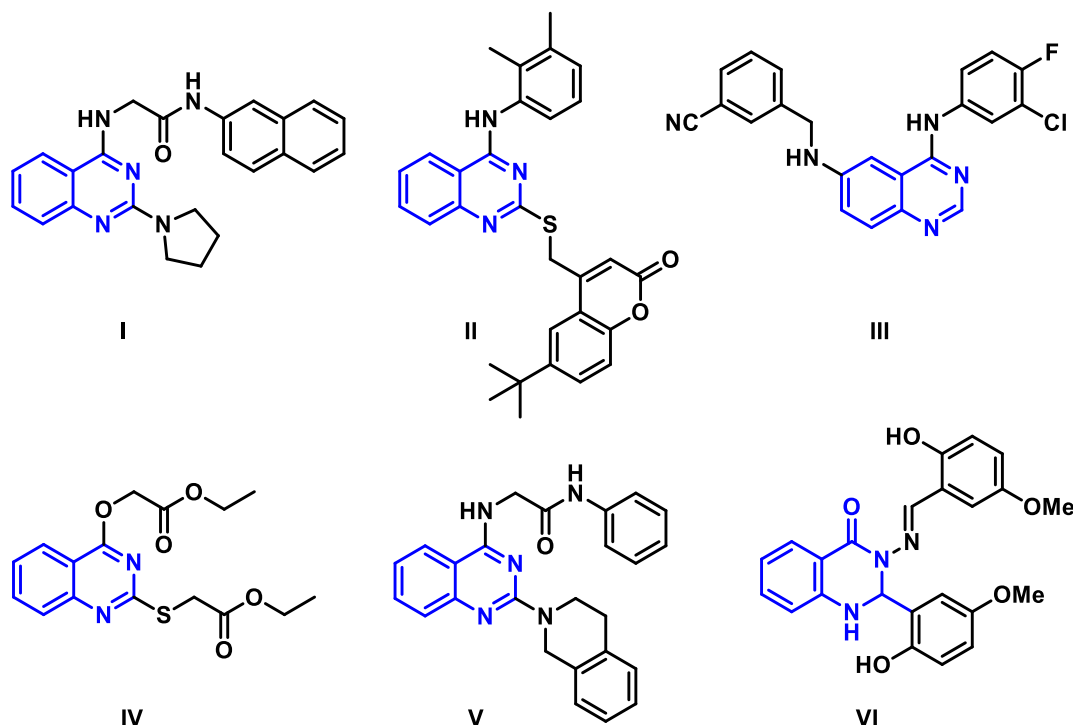


Fig. 1. Examples of antiviral agents I-VI incorporating quinazoline scaffold.

for the design of promising antiviral agents against SARS-CoV-2 as they play a key role in the life cycle of SARS-CoV-2 virus with no homologues proteins in human cells [11–14]. Hence, inhibition of M^{pro} and/or PL^{pro} can result in a selective antiviral activity without side effects on humans [12].

In this context, quinazolines are regarded as one of the most interesting scaffolds for designing antiviral agents [15,16]. Quinazolines were reported to possess potential antiviral activity against diverse types of RNA viruses including respiratory syncytial virus (RSV) [17], influenza A virus (IAV) [18] as well as hepatitis C virus (HCV) [19]. For instance, Zhang and co-workers [18] reported the design of a series of 2,4-disubstituted quinazoline derivatives incorporating *S*-acetamide and *NH*-acetamide moieties at position 4. Compound **I**, a representative of this series, was found to have a potent antiviral activity against IAV. Moreover, Hwu et al., [19] described the potent antiviral activity of a class of quinazoline-coumarin conjugates, for example compound **II** showed potent antiviral activity against hepatitis C virus and chikungunya virus. Meanwhile, Lee et al. [20] reported the synthesis of a series of 4-anilino-6-aminoquinazolines as anti-MERS-CoV inhibitors, compound **III**, a representative example of the synthesized series, showed $IC_{50} = 0.157 \mu M$, $CC_{50} = 3.59 \mu M$ and $SI = 25$. Recently, some studies reported the activity of quinazoline derivatives against SARS-CoV-2 [21,22]. For example, Zhao et al. [21] reported the promising activity of a series of quinolone and quinazoline derivatives in inhibiting RNA synthesis driven by SARS-CoV-2 RdRp. For instance, compounds **IV** and **V** revealed 58.43% and 58.83% inhibition on SARS-CoV-2 RdRp at $10 \mu M$ concentration. Additionally, Rothan and Teoh [22] reported the expected interesting potential of quinazoline derivatives, for example compound **VI**, in inhibiting SARS-CoV-2 Main Protease (M^{pro}) in a high throughput virtual screening campaign (Fig. 1).

On the other hand, several studies reported the promising antiviral properties of various heterocycles substituted with *N*-aryl-2-(thio)acetamide moieties. For instance, RDEA806 (**VII**) was reported to possess a potential HIV-1 reverse transcriptase (RT) inhibitory

activity against wild-type (WT) as well as some non-nucleoside reverse transcriptase (NNRT) resistant viruses [23]. Moreover, Zhan and co-workers [24] reported the synthesis and the interesting antiviral properties of novel 1,2,4-triazin-6-yl-thioacetamide derivatives as potent HIV-1 NNRTIs. Compound **VIII** was an example of this series displaying nanomolar activity against HIV-1(WT) as well as a moderate potency against the double mutant strain RES056. Furthermore, Zhang et al. [25] reported the discovery of some indol-3-yl-thio-*N*-phenyl-acetamides with potent antiviral activity. For instance, compound **IX** revealed a dual potency against RSV and IAV [25]. Moreover, Yu et al. [26] reported the potent anti-influenza activity of different pyrimidines substituted at 2 position with a *N*-aryl-2-(thio)acetamide moiety. For example, compound **X** demonstrated a broad activity against IAV and IBV. In addition, Zhan and co-workers [27] reported the anti-influenza properties of some thiazolyl-*N*-aryl-2-(thio)acetamides, for example, the derivative **XI** displayed a potent activity on influenza A/H1N1 virus (Fig. 2).

Rationale design of thioquinazoline-*N*-aryl-acetamide/*N*-arylaceto-hydrazide hybrids

Encouraged by the previous findings, and since most of the antiviral drugs in the clinical use were not designed specifically for SARS-CoV-2, we were interested in the current study in designing a new series of anti-SARS-CoV-2 through the application of the molecular hybridization strategy between the quinazoline ring and the *N*-aryl-2-(thio)acetamide moiety to design a novel series of (tetrahydro)thioquinazoline-*N*-arylaceto-hydrazide hybrids **XII** (Fig. 3). For further structure-activity relationship investigation, further elongation of the *N*-aryl-2-(thio)acetamido linkage was carried out by its replacement with a 2-(thio)acetohydrazide linker to afford scaffold **XIII** (Fig. 3). Derivatives from the designed scaffolds were synthesized utilizing the conventional methods of organic chemistry. Subsequently, the synthesized compounds were assayed for their antiviral activity against SARS-CoV-2. Promising hits were further examined for their expected mode of antiviral activity. Additionally, their physicochemical as well as pharmacoki-

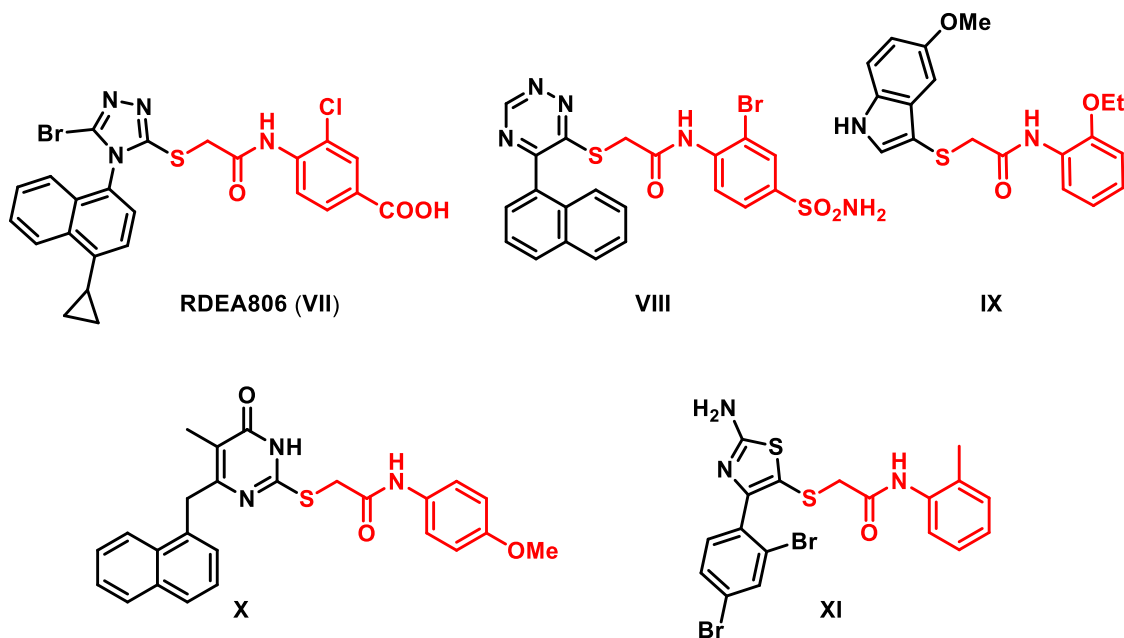


Fig. 2. Structures of antiviral agents VII-XI incorporating *N*-aryl-2-(thio)acetamide moiety.

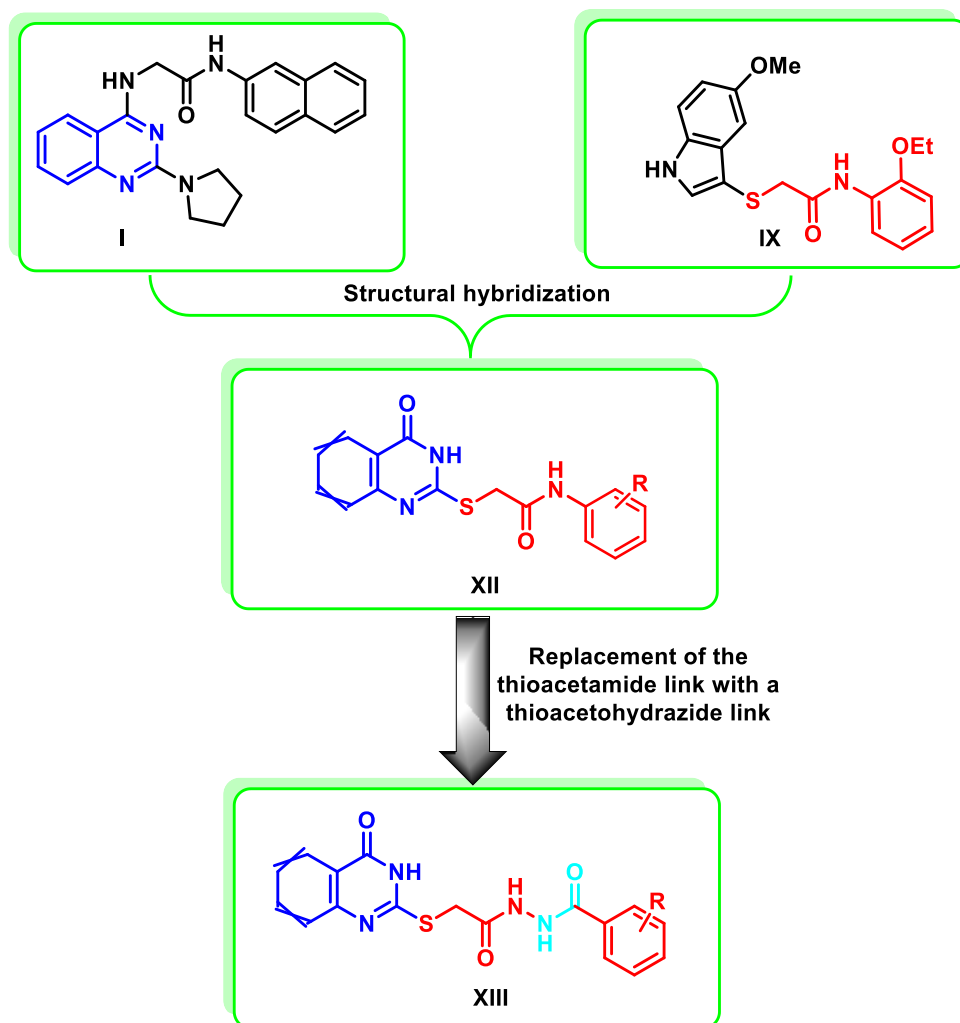
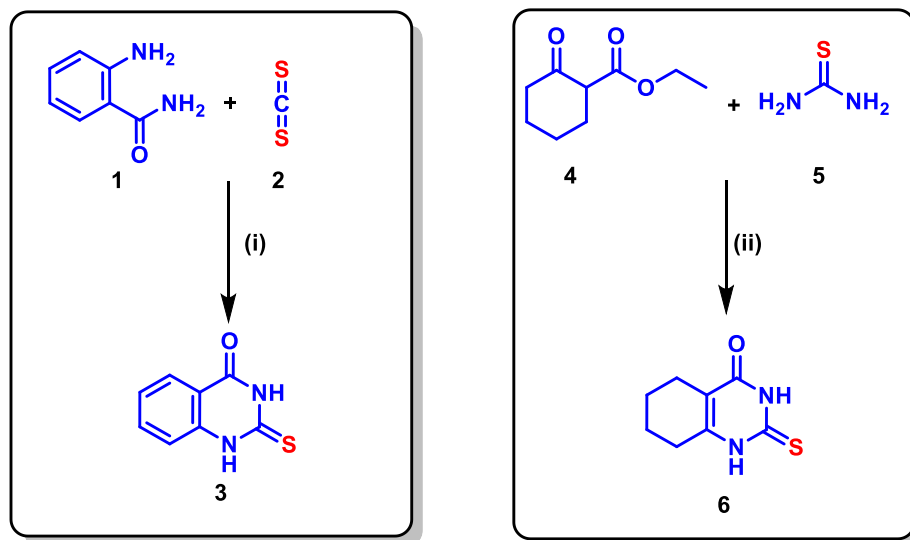


Fig. 3. The design strategy of the target (tetrahydro)thioquinazoline-*N*-arylacetamides XII and (tetrahydro)thioquinazoline-*N*-arylacetohydrazides XIII as anti-SARS-CoV-2 agents.



Reagents and conditions: (i) KOH, EtOH, H₂O, 30 °C, 21h; (ii) KOH, EtOH, reflux, 6h

Scheme 1. Synthesis of the starting quinazolines 3 and 6.

netic properties were predicted using the SwissADME free webtool. Concurrently, *in silico* molecular docking studies were performed in the SARS-CoV-2 Main Protease (M^{Pro}) binding site to study their binding mode in order to rationalize their promising antiviral activity.

2. Results and discussion

2.1. Chemistry

Initially, the starting quinazoline 3 was synthesized by the reaction of 1 with CS₂ (2) in the presence of KOH at 30 °C [28,29]. Meanwhile, the starting material 6 was synthesized by the condensation of 4 with thiourea (5) under basic conditions [30,31] (Scheme 1).

For the synthesis of the target compounds 11a-c and 12a-c; 2-aminobenzoic acid (7a), 3-aminobenzoic acid (7b), and 4-aminobenzoic acid (7c) were reacted with chloroacetyl chloride (8) in DMF to afford the intermediates 9a-c, respectively, which were subsequently reacted with the starting materials 3 and 6 under basic conditions to afford the target compounds 11a-c and 12a-c, respectively, in excellent yields (Scheme 2).

For the synthesis of the target quinazolines 17 and 18, different benzoic acid derivatives 13 were first esterified to give the corresponding esters 14 which were subsequently reacted with hydrazine hydrate to afford the corresponding acid hydrazides 15 (Scheme 3). Further reaction of 15 with chloroacetyl chloride (8) was performed to give the intermediates 16 which were reacted with the thioquinazolines 3 and 6 to yield the target compounds 17 and 18, respectively, in excellent yields.

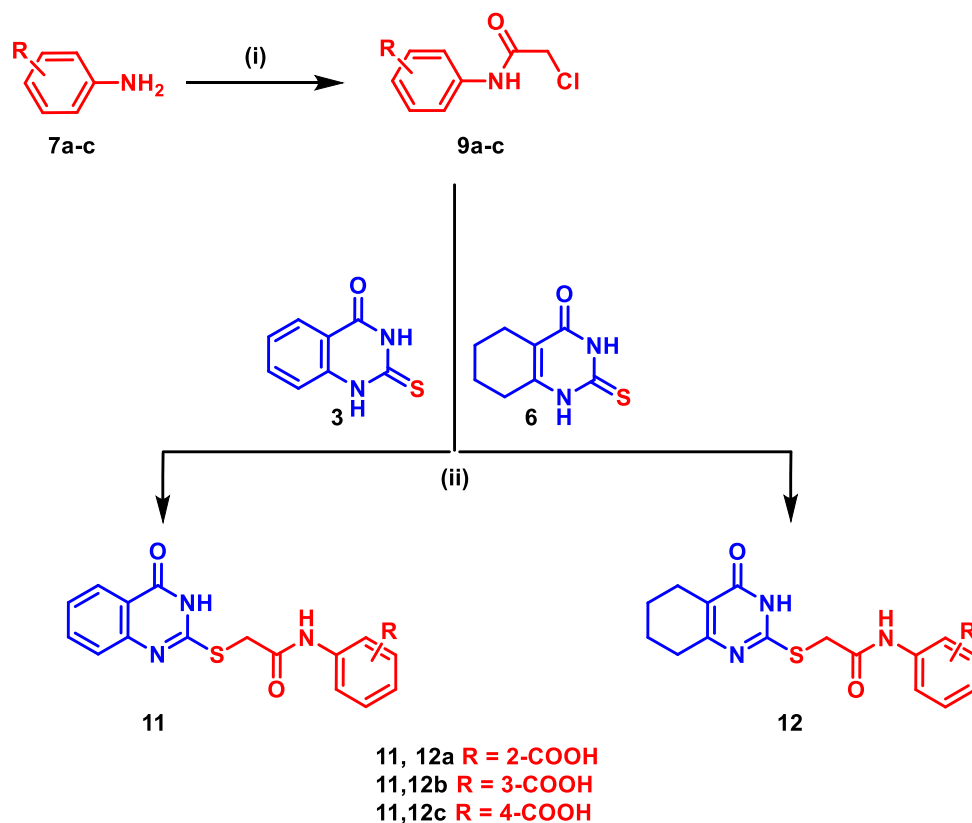
2.2. Biological evaluation

All the target compounds 11a-c, 12a-c, 17a-g and 18a-g were evaluated for their antiviral activity against NRC-03-nhCoV as well as for their cytotoxic activity on Vero-E6 cells employing MTT assay [32]. The CC₅₀ (concentration necessary for 50% growth inhibition of normal cell line compared to the control experiment) of the target compounds on Vero-E6 cells and IC₅₀ (concentration necessary for 50% reduction of virus-induced cytopathic effect

(CPE) compared to the virus control experiment) of the target compounds against NRC-03-nhCoV virus in Vero-E6 cells are presented in Table 1. The selectivity indices which are the ratio of CC₅₀ relative to IC₅₀ of the tested compounds were calculated and depicted in Table 1. In addition, Fig. 4 presents the inhibition curves of the most potent compounds 17g, 18c, and 18f (For the rest of the inhibition curves see the SI).

The presented study showed promising activity in comparison to the results reported in the literature [20,21]. From the IC₅₀ results presented in Table 1, it is obvious that the synthesized thioquinazolines and tetrahydrothioquinazolines displayed moderate to potent antiviral activity against NRC-03-nhCoV. Compounds 17g, 18c and 18f showed the most potent inhibitory activity with IC₅₀ of 21.4, 38.45 and 26.4 μM, respectively, on NRC-03-nhCoV. Close investigation of the antiviral results revealed that the thioquinazoline-*N*-aryl-acetamide hybrids 11a-c demonstrated moderate antiviral properties with an IC₅₀ range of 79.2 to 104 μM. Compounds 11b and 11c incorporating 3 and 4 carboxylic groups, respectively, showed higher potencies in comparison to the 2-carboxylic acid derivative 11a with IC₅₀ of 79.7, 79.2, and 104 μM, respectively, as well as higher SIs. Replacing the thioquinazoline moiety in series 11a-c with a tetrahydrothioquinazoline moiety in series 12a-c decreased the antiviral activity (IC₅₀ range of 173.6 to 531.3 μM). Compound 12a, with a carboxylic acid moiety at the 2 position, showed an IC₅₀ of 173.6 μM and a 2.5-fold higher selectivity toward the virus over the host cells (CC₅₀ = 431.4 μM). Shifting the COOH moiety to the 3 and 4 positions in 12b and 12c, respectively, resulted in more than a 2-fold decrease in the antiviral potency with no preferential selectivity (SI = 0.98 and 0.63, respectively).

Replacing the thio-*N*-aryl-acetamide moiety of series 11a-c with thioacetohydrazide moiety in series 17a-g, resulted in a different pattern of potency as well as specificity. The thioquinazoline-*N*-aryl-acetohydrazide derivative 17a with an unsubstituted terminal phenyl moiety displayed a weak antiviral activity (IC₅₀ = 317.5 μM) and high cytotoxic activity (CC₅₀ = 186.4 μM, SI = 0.59). Introduction of 4-Me and 4-NO₂ groups at the terminal phenyl in 17b and 17c increased the antiviral properties with IC₅₀ of 126.7 and 121.1 μM, respectively and SI of 2.14 and 2.61 μM, respectively. Moreover, the 2-OMe 17d and 2-chloro 17e derivatives demonstrated a



Reagents and conditions: (i) ClCOCH_2Cl (**8**), DMF, 0°C -rt, 30 min; (ii) Anhydrous K_2CO_3 , EtOH, reflux, 2h

Scheme 2. Synthesis of the target compounds **11** and **12**.

decrease in the antiviral activity with IC_{50} of 258.8 and 457.8 μM , respectively, with concomitant high cytotoxic (CC_{50} = 101.2 and 114.2 μM , respectively). Introduction of 4-chloro group at the terminal phenyl group in **17f** resulted in a more than 4-fold increase in the antiviral activity (IC_{50} = 74.3 μM) in comparison to **17a** (IC_{50} = 317.5 μM) with reduced cytotoxic activity (CC_{50} = 319 μM and SI = 4.30). Furthermore, the 2-bromo congener **17g** demonstrated the highest antiviral activity (IC_{50} = 21.4 μM) with 8.64 times higher selectivity towards the virus over the host cells (CC_{50} = 184.9 μM).

Hydrogenation of the fused phenyl group of the thioquinazolinone ring in series **17a-g** to afford the tetrahydrothioquinazolinone series **18a-g** increased the antiviral activity in all cases with the exception of compounds **18e** and **18g**. Compound **18a** with unsubstituted phenyl group displayed a moderate antiviral activity (IC_{50} = 140.2 μM) with a low SI of 1.68 (CC_{50} = 235 μM). Introduction of 4- NO_2 and 4-Cl groups at the terminal phenyl moiety to yield **18c** and **18f**, respectively, resulted in a more than three-fold increase in potency in comparison to **18a** with IC_{50} of 38.45 and 26.4 μM , respectively, in addition to a more than 10-fold higher selectivity toward the virus over the host cell (SI = 10.67 and 16.04, respectively). On the other hand, introduction of 4-Me, 2-OMe, 2-Br groups at the terminal phenyl moiety to give **18b**, **18d**, and **18g** showed a decrease in the antiviral activity with IC_{50} = 93.40 to 113.7 μM . Slight decrease in the antiviral activity was found for **18e** (IC_{50} = 459.8 μM) in comparison to **17e** (IC_{50} = 457.8 μM) and more than four-fold reduction was observed for 2-bromo derivative **18g** (IC_{50} = 93.40 μM) in comparison to **17g** (IC_{50} = 21.4 μM).

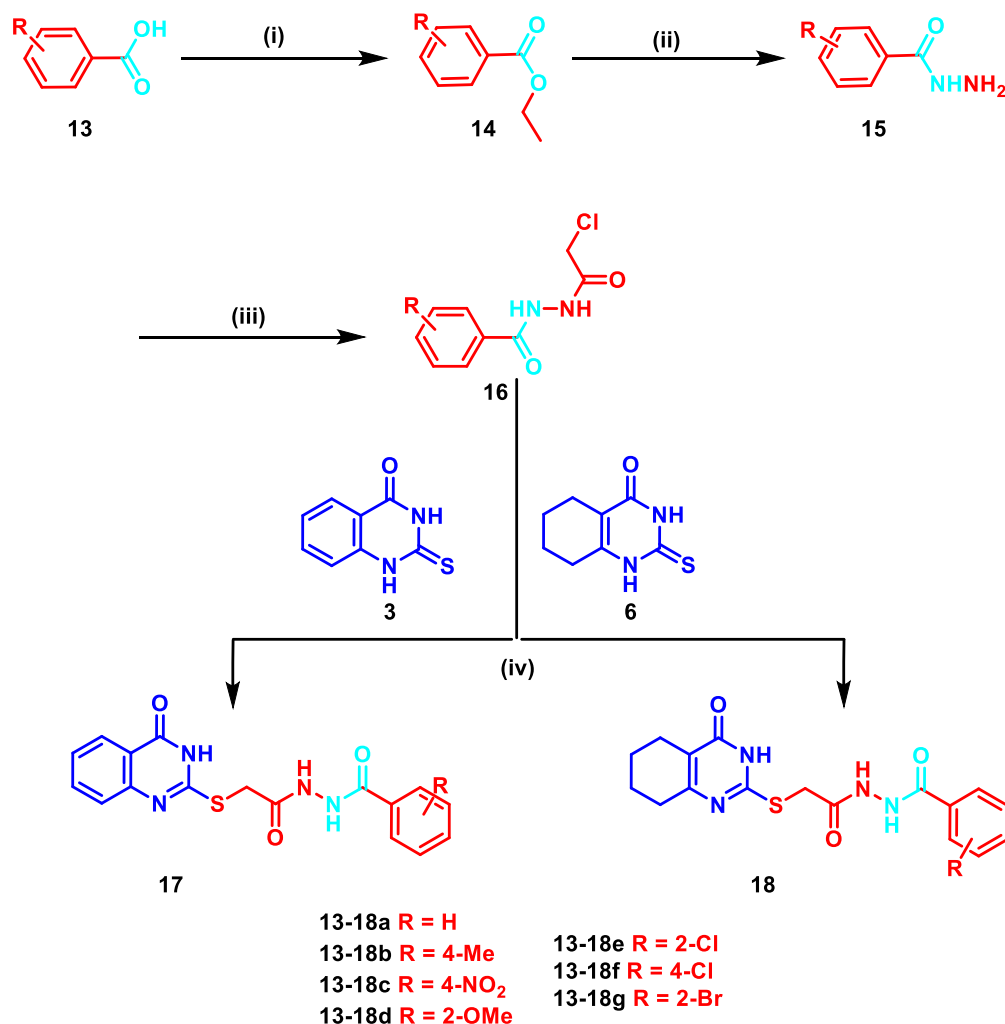
In summary, although compound **17g** displayed the highest antiviral activity with IC_{50} of 21.4 μM , it was less favored because

of its cytotoxic properties (CC_{50} = 184.9 μM and SI = 8.64). On the contrary, **18f** and **18c** were regarded to be the most promising derivatives in terms of their potency (IC_{50} = 26.4 and 38.45 μM) as well as their selectivity and safety (SI = 16.04 and 10.67).

2.3. Mechanism of Anti-SARS-CoV-2 Activity

For further investigation of the mechanism of virus inhibition of the most promising derivatives **17g**, **18c** and **18f**, a plaque infectivity reduction assay was performed [34]. This assay studied whether the promising derivatives affected the virus at the adsorption stage and/or replication stage and/or due to their direct virucidal effect. The inhibition results are depicted in Table 2. Interestingly, the three derivatives were found to have multiple inhibitory effects to different extents in the three stages. Nevertheless, the replication stage was found to be the most affected following treatment with the tested compounds (40-50% viral inhibition at 125 μM and 38.9-40% viral inhibition at 62.5 μM).

As can be seen in Table 2, the thioquinazolinone-*N*-aryl acetamide derivative **17g** showed at 125 μM a moderate inhibition of the virus at the adsorption stage 29.6%, whereas it showed a potent inhibition at the replication stage (50%) as well as a potent virucidal effect (47.8%). The tetrahydrothioquinazolinone-*N*-arylaceto-hydrazide **18c** displayed moderate inhibitory activity on the three tested mechanisms. At 125 μM , it revealed inhibition% of 44.4 and 43.3% by applying adsorption and replication mechanisms, respectively, and a 38.9% virucidal effect was noticed. Moreover, at 125 μM , compound **18f** was found to have 53% virucidal activity as well as a 40% inhibitory effect on virus replication and only 20% inhibition of the viral adsorption mechanism.



Reagents and conditions: (i) conc.H₂SO₄, EtOH, reflux, 2h; (ii) NH₂NH₂.H₂O, EtOH, reflux, 2h; (iii) ClCOCH₂Cl (8), DMF, 0 °C-rt, 30 min; (iv) Anhydrous K₂CO₃, EtOH, reflux, 2h

Scheme 3. Synthesis of the target compounds **17** and **18**.

2.4. Molecular modeling

Protease enzyme plays a critical role in viral protein maturation by cleaning proproteins after their translation into the host cell cytosol. As a result, viral proteases are considered potential antiviral drug targets [35]. The inhibition of a viral protease can reduce the assembly of mature viral particles. Therefore, SARS-CoV-2 main protease (M^{Pro}) could be a plausible target for the newly synthesized compounds, especially with its reported pyrimidinedione inhibitors which are analogues to our designed antiviral derivatives [36], thus, molecular docking simulations have been carried out to study the binding pattern of the target compounds **11a-c**, **12a-c**, **17a-g**, and **18a-g** in the active site of SARS-CoV-2 main protease (M^{Pro}). For this end, the X-ray crystallographic structure of SARS-CoV-2 main protease (M^{Pro}) co-crystallized with a pyrimidine-2,4-dione inhibitor (YD1) (PDB ID: 7LTJ) [36]. The molecular docking protocol was first validated by self-docking of the co-crystallized ligand (YD1) in the vicinity of the enzyme active site. The self-docking step reproduced the co-crystallized ligand pose efficiently with a docking score (S) of -13.26 kcal/mol and a root mean

square deviation (RMSD) of 1.538 Å. Moreover, the docking protocol reproduced all the key interactions with the active site amino acids (Figs. 5 and 6). Using the validated molecular docking protocol, the target compounds **11a-c**, **12a-c**, **17a-g**, and **18a-g** were docked in the SARS-CoV-2 M^{Pro} active site.

Generally, the target compounds showed a common binding pattern in the target enzyme (M^{Pro}) active site accommodated in subsites S1 and S2 (Figs. 7–9). The (tetrahydro)quinazolinone moiety occupies YD1 uracil binding subsite S1 driven by polar contacts interacting by its carbonyl group with the key amino acid His163 through hydrogen bonding. On the other side, the substituted phenyl group occupies the largely hydrophobic S2 subsite occupied by YD1 dichlorophenyl moiety. The target compounds' substituted phenyl group is stabilized through π - π stacking with the imidazole side chain of the key catalytic amino acid His41. The substituted phenyl group is sandwiched between the side chains of the amino acids His41 and Gln189. The linker in-between interacts through multiple H-bond interactions with the surrounding key amino acids Asn142, Gly143, Cys145, and His164. In compounds **11a-c** and **12a-c**, the peripheral carboxylate moiety on the distal phenyl group is involved in extra hydrogen bond interactions

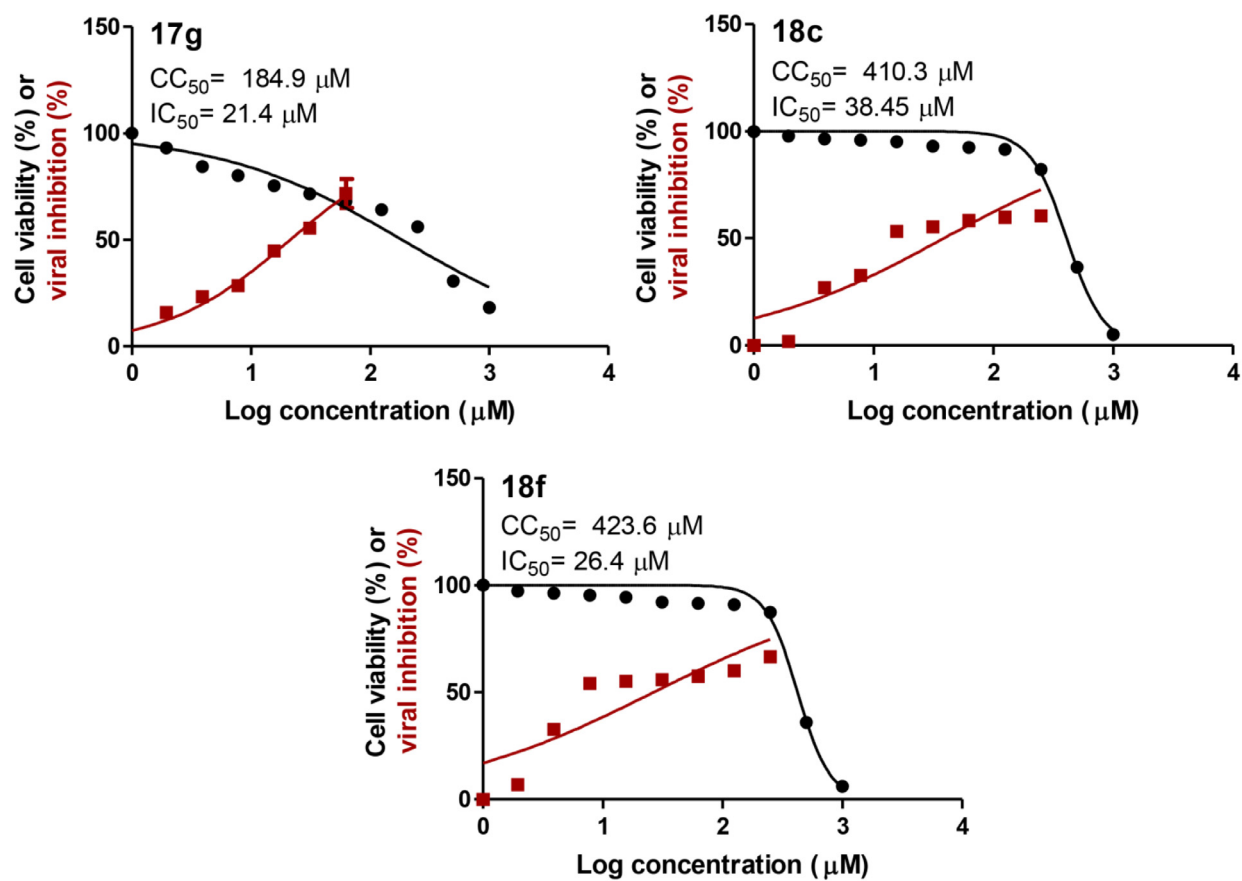


Fig. 4. Dose-inhibition curves of **17g**, **18c**, and **18f** against NRC-03-nhCoV [33] and Vero-E6 cells; IC_{50} and CC_{50} values were calculated using nonlinear regression analysis of GraphPad Prism software (version 5.01) by plotting log inhibitor versus normalized response (variable slope).

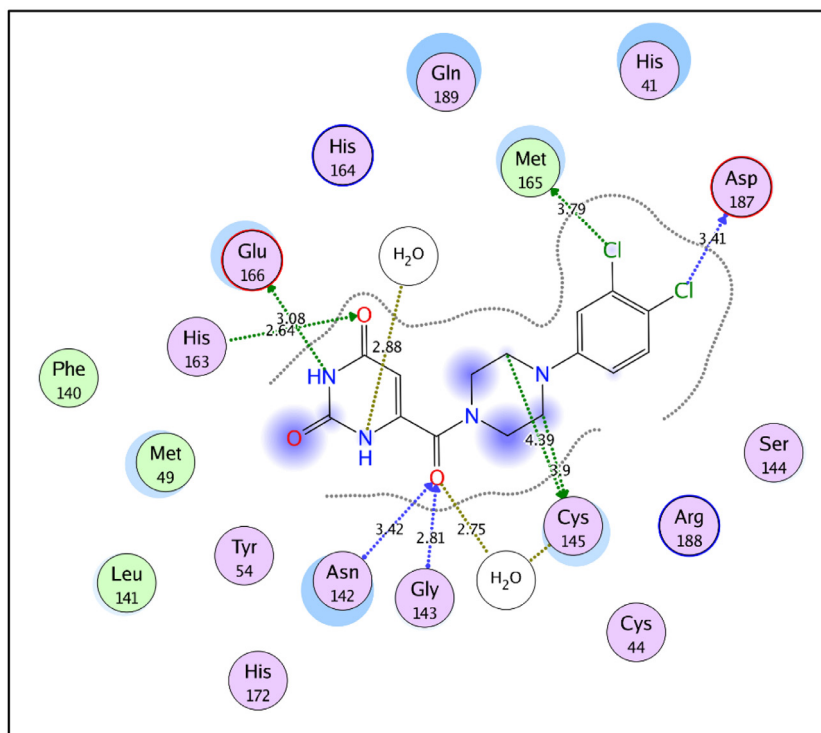
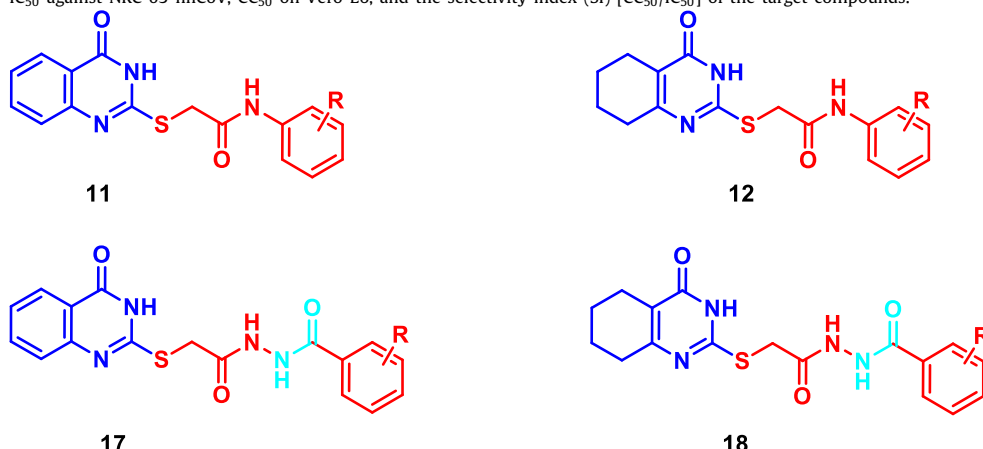


Fig. 5. 2D interaction diagram of the co-crystallized inhibitor **YD1** in M^{pro} active site (PDB ID: 7LTJ).

Table 1
IC₅₀ against NRC-03-nhCoV, CC₅₀ on Vero-E6, and the selectivity index (SI) [CC₅₀/IC₅₀] of the target compounds.



Compound ID	R	IC ₅₀ ^a (μM)	CC ₅₀ ^b (μM)	SI ^c
11a	2-COOH	104	450.5	4.3
11b	3-COOH	79.7	394	4.9
11c	4-COOH	79.2	442.6	5.6
12a	2-COOH	173.6	431.4	2.5
12b	3-COOH	531.3	524.3	0.98
12c	4-COOH	530.4	333.5	0.63
17a	H	317.5	186.4	0.59
17b	4-Me	126.7	271.4	2.14
17c	4-NO ₂	121.1	316.1	2.61
17d	2-OMe	258.8	101.2	0.4
17e	2-Cl	457.8	114.2	0.24
17f	4-Cl	74.3	319	4.3
17g	2-Br	21.4	184.9	8.64
18a	H	140.2	235	1.68
18b	4-Me	113.7	503.8	4.43
18c	4-NO ₂	38.45	410.3	10.67
18d	2-OMe	107	315.5	2.95
18e	2-Cl	459.8	524.5	1.14
18f	4-Cl	26.4	423.6	16.04
18g	2-Br	93.4	488.8	5.23

^aIC₅₀ (half maximal inhibitory concentration); ^bCC₅₀ (half maximal cytotoxic concentration); ^cSI (Selectivity index).

Table 2
Mechanisms of action of **17g**, **18c** and **18f** against SARS-CoV-2.

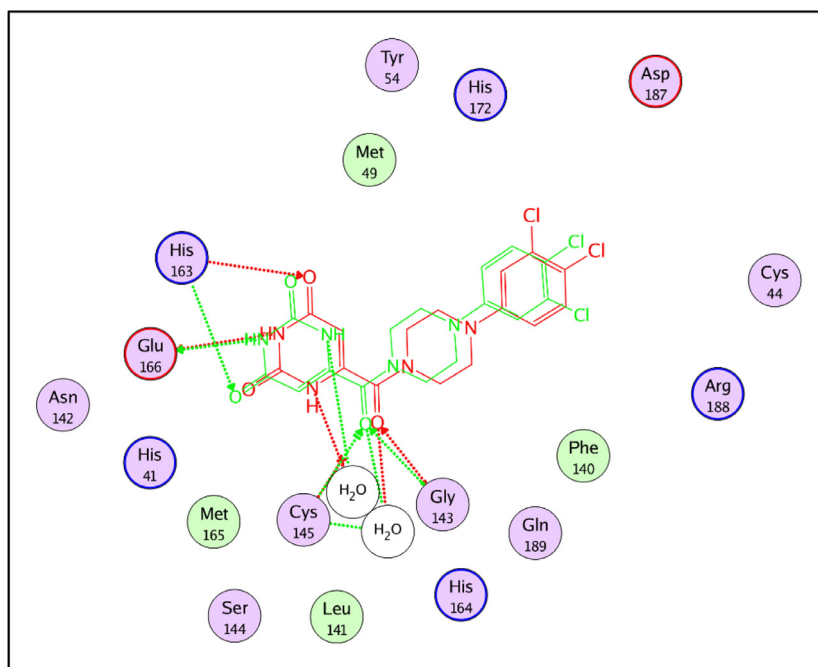
Compound ID	Conc (μM)	Mode of action Virus inhibition%		
		Adsorption	Replication	Virucidal
17g	125	29.6 ± 8.3	50.0 ± 3.3	47.8 ± 5.1
	62.5	26.7 ± 6.65	45.1 ± 1.71	37.3 ± 6.43
	31.25	16.7 ± 3.35	38.2 ± 4.29	25.6 ± 5.1
18c	125	44.4 ± 3.87	43.3 ± 3.35	38.9 ± 2.31
	62.5	28.9 ± 10.18	38.9 ± 1.91	33.6 ± 6.03
	31.25	20.0 ± 3.3	30.0 ± 3.3	22.2 ± 5.1
18f	125	20.0 ± 3.3	40.0 ± 10	53.3 ± 3.35
	62.5	13.3 ± 3.35	40.0 ± 3.3	34.4 ± 5.1
	31.25	6.7 ± 6.65	31.6 ± 4.27	15.6 ± 13.89

with the amino acids His41, Cys44, Met49, Pro52, and/or Met165 (For further details see supporting materials).

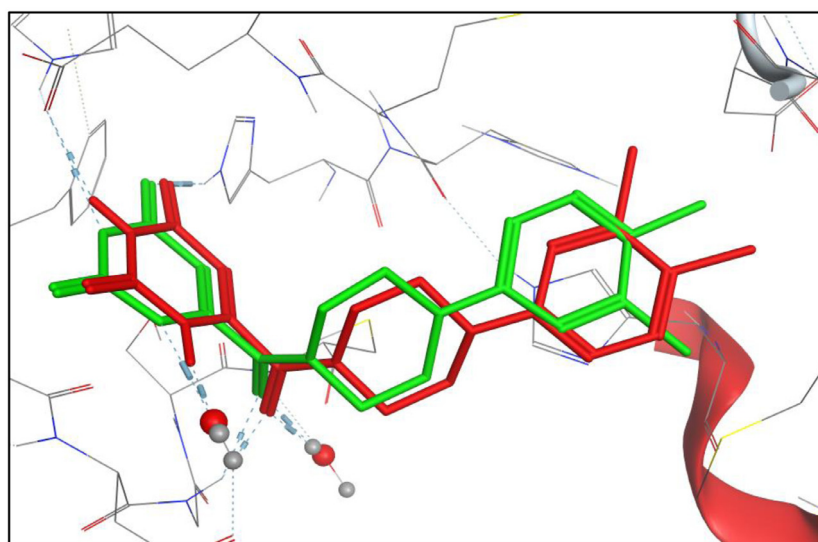
Table 3 shows the docking score of the target compounds and the co-crystallized ligand (**YD1**). The newly synthesized compounds show a predicted docking score range of −13.99 to −11.73 kcal/mol, whereas the co-crystallized ligand **YD1** showed a predicted docking score of −13.26 kcal/mol. As for the most promising compounds **17g**, **18c**, and **18f**, compound **18c** showed the most negative docking score −13.99 kcal/mol more negative than that of **YD1**. Whereas compounds **17g** and **18f** exhibited comparable

docking score (−12.45 and −12.07 kcal/mol, respectively) which is less negative than that of the co-crystallized ligand (**YD1**) (−13.26 kcal/mol) indicating their less predicted binding affinity than **YD1**. Compounds **17d**, **18a**, **17a**, and **17e** showed the least negative predicted docking scores (−11.54, −11.47, −11.38, and −11.37 kcal/mol) which agree with their poor experimental activity (258.8, 140.2, 317.5, and 457.8 μM).

The predicted binding pattern of the target compounds could rationalize their differential activity based on their hydrophobic interaction and fitting in the hydrophobic S2 subsite of the bind-



(A)

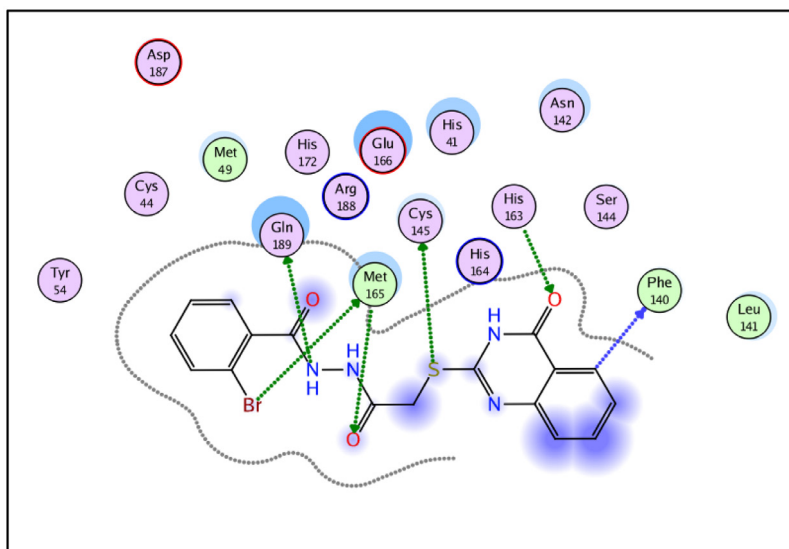


(B)

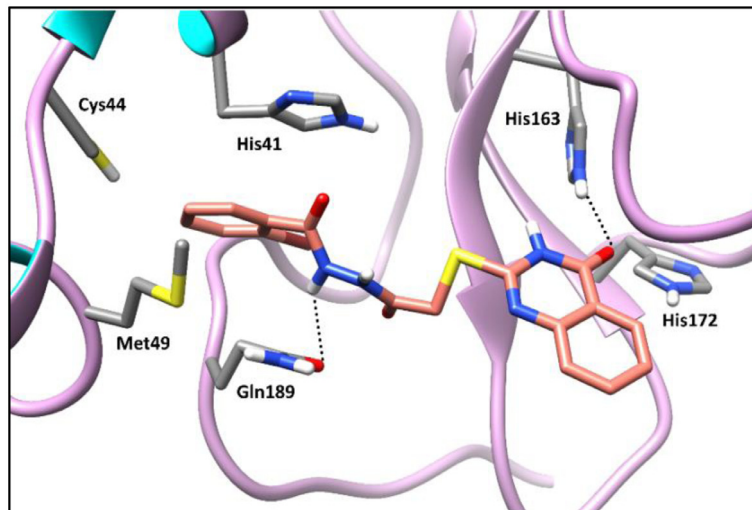
Fig. 6. 2D diagram (A) and 3D representation (B) of the superimposition of the co-crystallized (red) and the docking pose (green) of **YD1** in the active site of M^{pro} (PDB ID: 7LTJ).

ing site. Compounds **11a-c** and **12a-c** showed a relatively less predicted binding affinity due to their ionic polar carboxylate substitution on their distal phenyl group which decreases the probable hydrophobic interactions with the hydrophobic S2 subsite, however, this loss of proper hydrophobic interactions is somehow compensated by the carboxylate involvement in multiple extra hydrogen bond interactions with the amino acids His41, Cys44, Met49, Pro52, and/or Met165 like in case of compound **11b**. On the other hand, compounds **17a-g** and **18a-g** show better predicted binding affinity because of their hydrophobic substitutions on the distal phenyl group and the longer thioacetohydrazide linker which makes the (substituted)phenyl group better fitted

in the hydrophobic S2 subsite. Compounds achieving higher hydrophobic interaction with S2 subsite and better fit of their (substituted)phenyl group show strong predicted binding affinity as reflected in their promising experimental activity e.g., compounds **17g**, **18c**, and **18f** with *o*-bromo, *p*-nitro, and *p*-chloro substitution, respectively. Alternatively, compounds with unsubstituted distal phenyl ring **17a** and **18a** show less predicted binding affinity relative to their substituted congeners due to their less possible hydrophobic interactions with S2 subsite. Compounds with less hydrophobic substituents (OMe) e.g., compounds **17d** or that are not well fitted in the S2 subsite e.g., compounds **17e** and **18e** show weaker predicted binding affinity which is reflected



(A)



(B)

Fig. 7. 2D diagram (A) and 3D representation (B) of compound **17g** showing its interaction in M^{pro} active site (PDB ID: 7LTJ).

in their weak experimental activity ($IC_{50} = 258.8, 457.8,$ and $459.8 \mu M$).

2.5. Estimation of physicochemical, pharmacokinetic and ADME properties

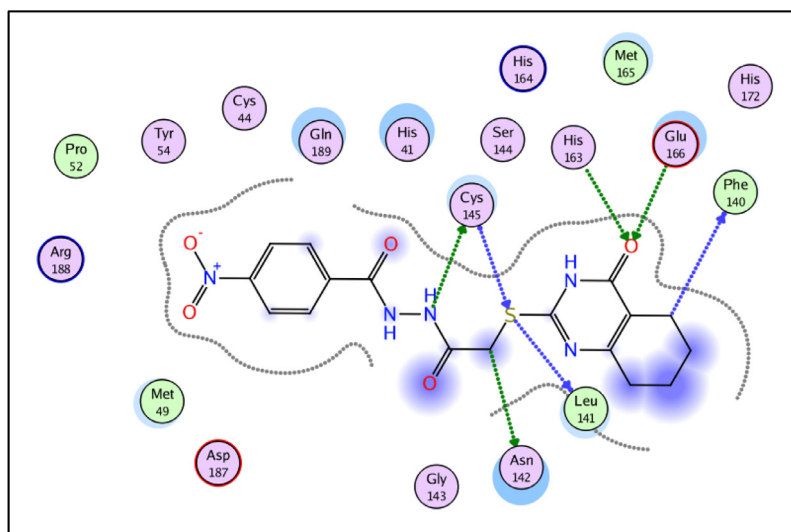
Encouraged by the promising antiviral properties of **17g**, **18c** and **18f**, they were further selected to predict their physicochemical and ADME properties using SwissADME free web tool [37]. Table 4 presents some selected results of **17g**, **18c** and **18f**.

Analysis of the obtained results (Table 4) revealed that the target thioquinazoline-*N*-aryl acetamide **17g** and tetrahydrothioquinazoline-*N*-aryl acetohydrazides **18c** and **18f** express acceptable levels of physicochemical properties. The molecular weight of **17g**, **18c** and **18f** is spanning between 392.86 to 433.28 g/mol. They incorporate acceptable numbers of hydrogen bond donors (less than 5) and acceptors (less than 10). Additionally, the topological polar surface area (TPSA) for **17g** and **18f** is

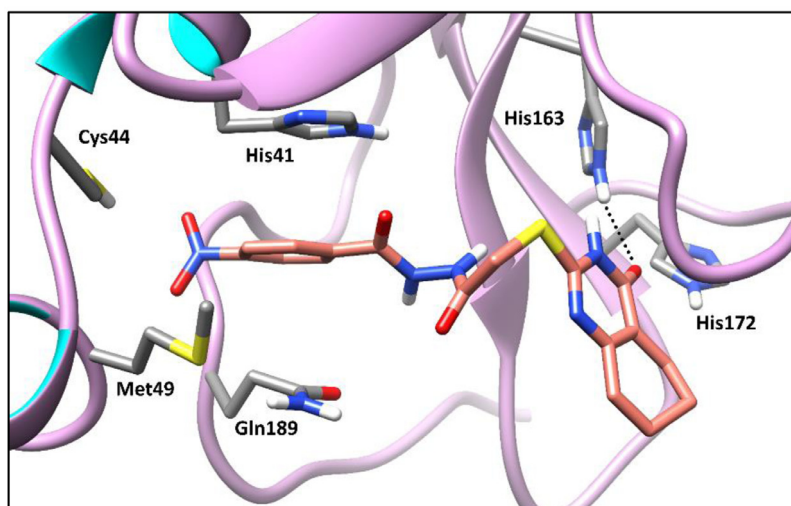
129.25 Å, while it is slightly high in case of the **18c** $TPSA = 175.07$ Å and the $ilogP$ (octanol-water partition coefficient) is ranging from 1.60 to 2.62 [38].

The target (tetrahydro)thioquinazoline-*N*-arylacetamides **17g** and **18f** are predicted to be well absorbed from the GIT while **18c** is predicted to have low GIT absorption. The three target compounds **17g**, **18c** and **18f** have no predicted ability to penetrate the blood brain barrier which decreases their probable adverse effect at the central level. Compounds **18c** and **18f** were found to be substrates for P-glycoprotein (P-gp), which plays a significant role in the removal of strange substances outside the cells. Meanwhile, **17g** is not a substrate for P-glycoprotein (P-gp) [39].

Fig. 10 presents the bioavailability radar chart of compounds **17g**, **18c** and **18f** provided by the SwissADME web tool [37]. Generally, the bioavailability radar presented by SwissADME demonstrates a pink-colored area that identifies the optimum space of six physicochemical parameters for oral bioavailability. These six properties are size, polarity, lipophilicity, solubility, flexibility, and sat-



(A)



(B)

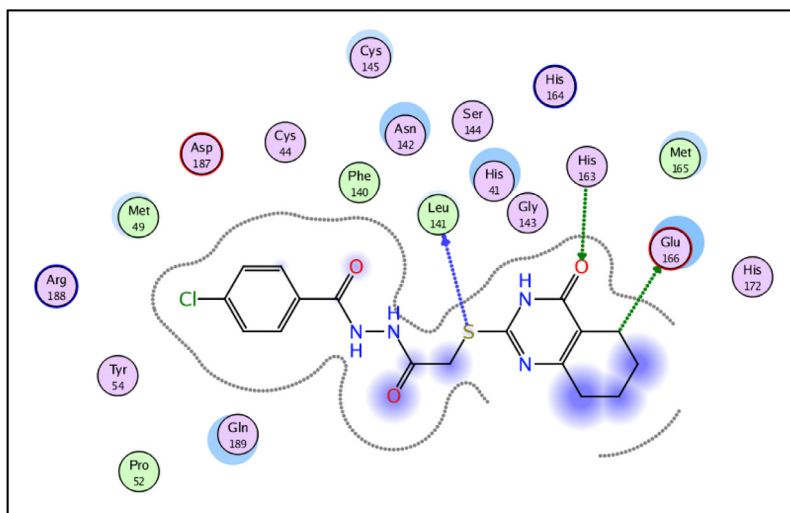
Fig. 8. 2D diagram (A) and 3D representation (B) of compound **18c** showing its interaction in M^{pro} active site (PDB ID: 7LTJ).

uration. Close investigation of the presented radar charts showed that compound **18f** occupies the ideal space of the six physicochemical properties for oral bioavailability, whereas the derivatives **17g** and **18c** are nearly fully located in the pink area, only the degree of unsaturation slightly deviates from the optimum in **17g** while the polarity is slightly deviating from the ideal for **18c** (Fig. 10).

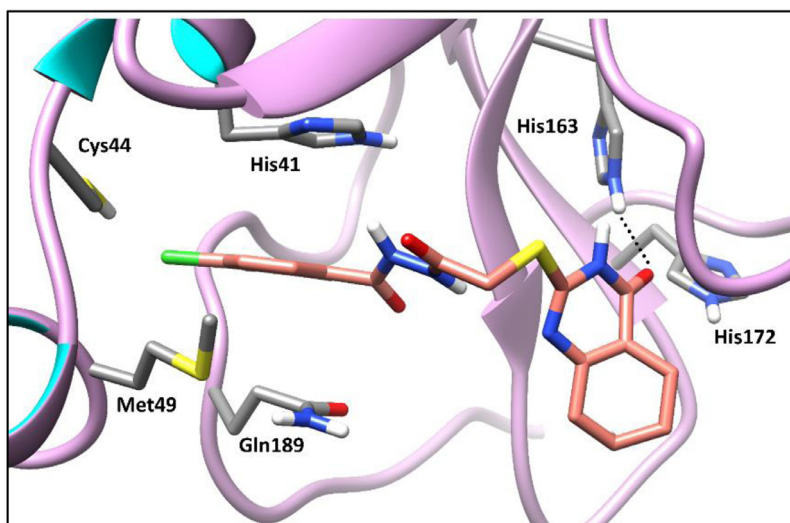
Moreover, it is attractive that **17g** and **18f** follow all rules of drug-likeness, they do not violate Lipinski's rule [40], Veber rule [41], Ghose-filter [42], Egan [43] or Muegge's filter [44]. Because of the high TPSA of compound **18c**, it satisfies only Lipinski's rule. In addition, it worth pointing out that the three derivatives do not incorporate in their structures Pan Assay Interference (PAINS) fragments [45]. Hence, in addition to the promising antiviral activity of the target compounds, their promising drug-likeness parameters suggests their potential to be subjected for future optimization for the discovery of chemotherapeutic agents.

3. Conclusion

The presented study involves the design, synthesis, and anti-SARS-CoV-2 activity evaluation of two novel series of (tetrahydro)thioquinazoline-*N*-arylacetamides and (tetrahydro)thioquinazoline-*N*-arylacethydrazides. The thioquinazoline-*N*-arylacetamide **17g** and the tetrahydrothioquinazoline-*N*-arylacethydrazides **18c** and **18f** showed potent antiviral activity with $IC_{50} = 21.4$, 38.45, and 26.4 μM , respectively. The derivatives **18c** and **18f** exhibited $SI = 10.67$ and 16.04, respectively, towards the virus over the host cells. In addition, the three derivatives **17g**, **18c**, and **18f** showed promising virucidal properties beside their ability to inhibit the virus at the adsorption as well as at the replication stages. Moreover, besides their promising antiviral activity, compounds **17g**, **18c** and **18f** displayed acceptable physicochemical and pharmacokinetic properties for further optimization as antiviral agents.



(A)



(B)

Fig. 9. 2D diagram (A) and 3D representation (B) of compound **18f** showing its interaction in M^{PO} active site (PDB ID: 7LTJ).

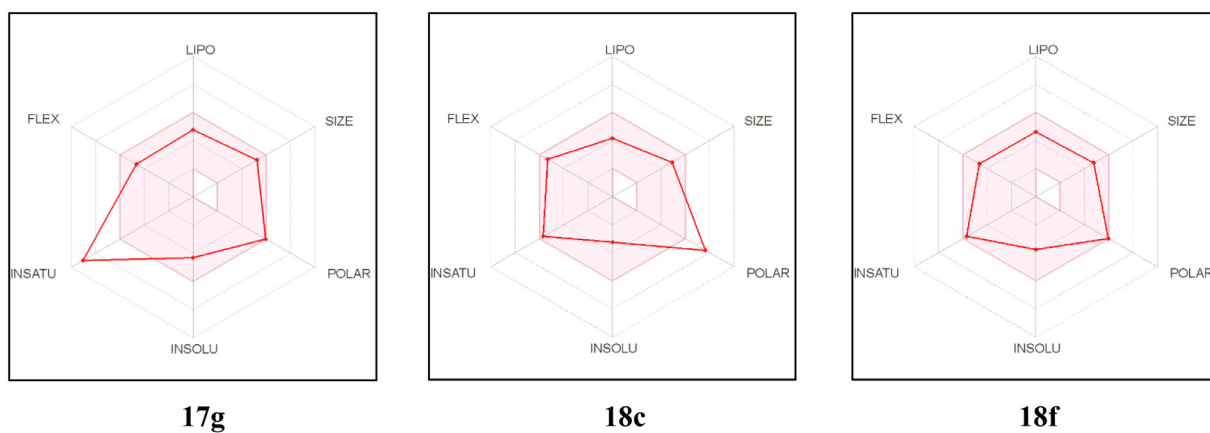


Fig. 10. Bioavailability radar plot from SwissADME online web tool for **17g**, **18c** and **18f**.

Table 3

Docking energy scores (*S*) in kcal/mol for the target compounds and the co-crystallized compound (YD1) in M^{pro} active site (PDB ID: 7LTJ).

Compound	Energy score (<i>S</i>) kcal/mol	IC ₅₀ (μM)
11a	-11.60	104
11b	-11.58	79.7
11c	-11.92	79.2
12a	-11.98	173.6
12b	-11.96	531.3
12c	-12.39	530.4
17a	-11.38	317.5
17b	-12.16	126.7
17c	-12.99	121.1
17d	-11.54	258.8
17e	-11.37	457.8
17f	-11.98	74.3
17g	-12.45	21.4
18a	-11.47	140.2
18b	-13.36	113.7
18c	-13.99	38.45
18d	-11.97	107
18e	-11.78	459.8
18f	-12.07	26.4
18g	-13.18	93.4
YD1	-13.26	4.2 [36]

Table 4

Selected calculated physicochemical and pharmacokinetic properties of **17g**, **18c** and **18f** from SwissADME free webtool [37].

Product	17g	18c	18f
MW	433.28	403.41	392.86
Rotatable bonds	7	8	7
H-bond acceptors	4	6	4
H-bond donors	3	3	3
MR	102.11	103.16	99.35
TPSA	129.25	175.07	129.25
iLogP	1.77	1.60	2.62
GI absorption	High	Low	High
BBB permeant	No	No	No
P-gp substrate	No	Yes	Yes

4. Experimental

4.1. Chemistry

4.1.1. General remarks

Chemicals along with solvents used for chemical reaction were obtained from commercial companies. Follow up of the reactions were carried out using analytical thin layer chromatography (TLC). Uncorrected melting points were recorded on a Stuart SMP30 melting point apparatus. Elemental analyses of the synthesized hybrids were recorded in the micro analytical labs, National Research Centre, Cairo, Egypt. IR spectra (4000–400 cm⁻¹) were recorded on Jasco FT/IR 300 E Fourier transform infrared spectrophotometer. ¹H NMR as well as ¹³C NMR spectra were measured in DMSO-*d*₆ as a solvent at 500 (125) MHz and 400 (100) MHz on Bruker instruments.

4.1.2. General procedure I for the synthesis of the target compounds **11a-c**, **12a-c**, **17a-g** and **18a-g**

A mixture of **3** or **6** and anhydrous K₂CO₃ was stirred for 30 min at room temperature then **3a-c** or **16a-g** was added and the mixture was heated under reflux for 2 h. The reaction mixture was then cooled to room temperature poured on ice and neutralized with few drops of 2N HCl and the precipitated product was filtered, dried and purified by crystallization from MeOH/ DCM 1:1

mixture to give the corresponding target products **11a-c**, **12a-c**, **17a-g**, **18a-g** in analytical pure form.

2-(2-((4-Oxo-3,4-dihydroquinazolin-2-yl)thio)acetamido)benzoic acid (**11a**)

Off white powder; yield = 95%; mp 250-252 °C; ¹H-NMR (500 MHz; DMSO-*d*₆) δ_H 4.15 (s, 2H), 7.13 (t, ³J = 7.5 Hz, 1H), 7.38 (t, ³J = 7.5 Hz, 1H), 7.46 (d, ³J = 8.0 Hz, 1H), 7.56 (t, ³J = 7.5 Hz, 1H), 7.69 (t, ³J = 7.5 Hz, 1H), 7.95 (d, ³J = 7.5 Hz, 1H), 8.00 (d, ³J = 7.5 Hz, 1H), 8.49 (d, ³J = 8.5 Hz, 1H), 11.77 (br., 1H), 12.47 (br., 1H), 12.76 ppm (br., 1H); ¹³C-NMR (125 MHz; DMSO-*d*₆) δ_C 35.08, 115.85, 116.70, 119.94, 122.92, 124.32, 125.79, 126.02, 131.13, 133.97, 134.56, 140.47, 148.22, 154.62, 161.17, 166.65, 169.34 ppm; Anal. Calcd for C₁₇H₁₃N₃O₄S: C, 57.46; H, 3.69; N, 11.82. Found: C, 57.73; H, 3.93; N, 11.65.

3-(2-((4-Oxo-3,4-dihydroquinazolin-2-yl)thio)acetamido)benzoic acid (**11b**)

Off white powder; yield = 87%; mp 252-254 °C; ¹H-NMR (400 MHz; DMSO-*d*₆) δ_H 4.19 (s, 2H), 7.40 (d, ³J = 7.2 Hz, 1H), 7.43 (t, ³J = 9.2 Hz, 1H), 7.63 (d, ³J = 7.6 Hz, 1H), 7.72 (dt, ³J = 7.8 Hz, ⁴J = 1.2 Hz, 1H), 7.80 (dd, ³J = 8.6 Hz, ⁴J = 1.2 Hz, 1H), 8.02 (d, ³J = 8.0 Hz, ⁴J = 1.2 Hz, 1H), 8.25 (s, 1H), 10.55 (s, 1H), 12.68 (br., 2H), 12.95 ppm (br., 1H); ¹³C-NMR (100 MHz; DMSO-*d*₆) δ_C 35.13, 115.86, 116.21, 119.91, 123.27, 124.28, 125.76, 126.10, 129.12, 131.39, 134.67, 139.18, 148.21, 155.26, 161.14, 166.24, 167.11 ppm; Anal. Calcd for C₁₇H₁₃N₃O₄S: C, 57.46; H, 3.69; N, 11.82. Found: C, 57.15; H, 3.87; N, 12.03.

4-(2-((4-Oxo-3,4-dihydroquinazolin-2-yl)thio)acetamido)benzoic acid (**11c**)

Pale yellow powder; yield = 83%; mp 249-251 °C; ¹H-NMR (400 MHz; DMSO-*d*₆) δ_H 4.11 (s, 2H), 7.29-7.40 (m, 2H), 7.68-7.69 (m, 2H), 7.88-7.89 (m, 2H), 7.99-8.00 (m, 2H), 11.06 (br., 2H), 12.45 ppm (br., 1H); Anal. Calcd for C₁₇H₁₃N₃O₄S: C, 57.46; H, 3.69; N, 11.82. Found: C, 57.64; H, 3.90; N, 11.66.

2-(2-((4-Oxo-3,4,5,6,7,8-hexahydroquinazolin-2-yl)thio)acetamido)benzoic acid (**12a**)

White powder; yield = 90%; mp 227-229 °C; ¹H-NMR (500 MHz; DMSO-*d*₆) δ_H 1.58-1.60 (m, 4H), 2.14-2.24 (m, 2H), 2.35-2.36 (m, 2H), 4.01 (s, 2H), 7.14-7.15 (m, 1H), 7.56-7.57 (m, 1H), 7.95-7.96 (m, 1H), 8.47 (d, ³J = 6.5 Hz, 1H), 11.61 (s, 1H), 12.71 ppm (br., 2H); ¹³C-NMR (125 MHz; DMSO-*d*₆) δ_C 21.35, 21.38, 21.67, 30.86, 34.97, 116.59, 116.67, 119.97, 122.88, 131.08, 133.96, 140.44, 155.90, 162.72, 166.71, 169.23 ppm; Anal. Calcd for C₁₇H₁₇N₃O₄S: C, 56.81; H, 4.77; N, 11.69. Found: C, 56.57; H, 4.45; N, 11.48.

3-(2-((4-Oxo-3,4,5,6,7,8-hexahydroquinazolin-2-yl)thio)acetamido)benzoic acid (**12b**)

White powder; yield = 81%; mp 263-265 °C; ¹H-NMR (400 MHz; DMSO-*d*₆) δ_H 1.61-1.62 (m, 4H), 2.24-2.25 (m, 2H), 2.39-2.40 (m, 2H), 4.04 (s, 2H), 7.41 (t, ³J = 8.0 Hz, 1H), 7.62 (d, ³J = 7.6 Hz, 1H), 7.76 (d, ³J = 8.0 Hz, 1H), 8.20 (s, 1H), 10.45 (s, 1H), 12.53 ppm (br., 1H); ¹³C-NMR (100 MHz; DMSO-*d*₆) δ_C 21.40, 21.72, 30.83, 34.95, 116.53, 119.92, 123.14, 124.24, 129.03, 131.72, 139.08, 156.49, 159.42, 162.79, 166.28, 167.28 ppm; Anal. Calcd for C₁₇H₁₇N₃O₄S: C, 56.81; H, 4.77; N, 11.69. Found: C, 56.62; H, 4.95; N, 11.47.

4-(2-((4-Oxo-3,4,5,6,7,8-hexahydroquinazolin-2-yl)thio)acetamido)benzoic acid (**12c**)

White powder; yield = 87%; mp 237-239 °C; ¹H-NMR (500 MHz; DMSO-*d*₆) δ_H 1.61-1.63 (m, 4H), 2.24-2.25 (m, 2H), 2.37-2.38

(m, 2H), 4.04 (s, 2H), 7.66 (d, $^3J = 8.0$ Hz, 2H), 7.88 (d, $^3J = 8.0$ Hz, 2H), 10.65 (s, 1H), 12.58 ppm (br., 2H); $^{13}\text{C-NMR}$ (125 MHz; DMSO- d_6) δ_{C} 21.95, 22.25, 31.30, 35.58, 116.98, 118.94, 126.38, 130.93, 143.27, 157.23, 163.56, 167.15, 167.71, 167.81 ppm; Anal. Calcd for $\text{C}_{17}\text{H}_{17}\text{N}_3\text{O}_4\text{S}$: C, 56.81; H, 4.77; N, 11.69. Found: C, 56.98; H, 4.53; N, 11.81.

N'-(2-((4-Oxo-3,4-dihydroquinazolin-2-yl)thio)acetyl)benzohydrazide (**17a**)

White powder; yield = 85%; mp 249–251 °C; $^1\text{H-NMR}$ (500 MHz; DMSO- d_6) δ_{H} 4.11 (s, 2H), 7.40–7.43 (m, 1H), 7.47–7.50 (m, 2H), 7.54–7.60 (m, 2H), 7.75–7.76 (m, 1H), 7.84–7.85 (m, 2H), 8.01–8.03 (m, 1H), 10.37 (br., 1H), 10.49 (br., 1H), 12.62 ppm (br., 1H); Anal. Calcd for $\text{C}_{17}\text{H}_{14}\text{N}_4\text{O}_3\text{S}$: C, 57.62; H, 3.98; N, 15.81. Found: C, 57.32; H, 4.15; N, 15.54.

4-Methyl-*N'*-(2-((4-oxo-3,4-dihydroquinazolin-2-yl)thio)acetyl)benzohydrazide (**17b**)

Pale yellow powder; yield = 91%; mp 243–245 °C; $^1\text{H-NMR}$ (500 MHz; DMSO- d_6) δ_{H} 2.34 (s, 3H), 4.11 (s, 2H), 7.27–7.28 (m, 2H), 7.42–7.43 (m, 2H), 7.60–7.61 (m, 1H), 7.76–7.77 (m, 2H), 8.02–8.04 (m, 1H), 10.31 (s, 1H), 10.41 (s, 1H), 12.69 ppm (br., 1H); $^{13}\text{C-NMR}$ (125 MHz; DMSO- d_6) δ_{C} 20.95, 32.10, 119.97, 125.75, 125.96, 126.20, 127.46, 128.92, 129.54, 134.56, 141.81, 148.26, 154.78, 161.13, 165.25, 166.56 ppm; Anal. Calcd for $\text{C}_{18}\text{H}_{16}\text{N}_4\text{O}_3\text{S}$: C, 58.68; H, 4.38; N, 15.21. Found: C, 58.45; H, 4.68; N, 15.57.

4-Nitro-*N'*-(2-((4-oxo-3,4-dihydroquinazolin-2-yl)thio)acetyl)benzohydrazide (**17c**)

Pale yellow powder; yield = 96%; mp 256–258 °C; $^1\text{H-NMR}$ (500 MHz; DMSO- d_6) δ_{H} 4.13 (s, 2H), 7.39–7.44 (m, 1H), 7.60 (t, $^3J = 6.5$ Hz, 1H), 7.76–7.78 (m, 1H), 8.02 (t, $^3J = 6.5$ Hz, 1H), 8.07–8.09 (m, 2H), 8.33–8.34 (m, 2H), 10.50 (s, 1H), 10.87 (s, 1H), 12.68 ppm (br., 1H); $^{13}\text{C-NMR}$ (125 MHz; DMSO- d_6) δ_{C} 32.05, 119.93, 123.64, 125.74, 125.97, 128.99, 134.53, 137.96, 148.21, 149.37, 154.87, 161.20, 163.78, 166.50 ppm; Anal. Calcd for $\text{C}_{17}\text{H}_{13}\text{N}_5\text{O}_5\text{S}$: C, 51.13; H, 3.28; N, 17.54. Found: C, 51.46; H, 3.55; N, 17.16.

2-Methoxy-*N'*-(2-((4-oxo-3,4-dihydroquinazolin-2-yl)thio)acetyl)benzohydrazide (**17d**)

White solid; yield = 85%; mp 224–226 °C; $^1\text{H-NMR}$ (500 MHz; DMSO- d_6) δ_{H} 3.86 (s, 3H), 4.10 (s, 2H), 7.05 (t, $^3J = 7.5$ Hz, 1H), 7.14 (d, $^3J = 8.5$ Hz, 1H), 7.42 (t, $^3J = 7.5$ Hz, 1H), 7.50 (dt, $^3J = 8.0$ Hz, $^4J = 1.5$ Hz, 1H), 7.58 (d, $^3J = 8.0$ Hz, 1H), 7.71 (dd, $^3J = 7.8$ Hz, $^4J = 1.5$ Hz, 1H), 7.76 (dt, $^3J = 7.5$ Hz, $^4J = 1.5$ Hz, 1H), 8.03 (dd, $^3J = 7.5$ Hz, $^4J = 1.0$ Hz, 1H), 10.08 (s, 1H), 10.65 (br., 1H), 12.71 ppm (br., 1H); $^{13}\text{C-NMR}$ (125 MHz; DMSO- d_6) δ_{C} 31.97, 55.93, 112.11, 119.94, 120.55, 121.14, 125.70, 125.97, 130.39, 132.80, 134.52, 148.15, 155.07, 156.99, 161.28, 163.39, 165.52 ppm; Anal. Calcd for $\text{C}_{18}\text{H}_{16}\text{N}_4\text{O}_4\text{S}$: C, 56.24; H, 4.20; N, 14.58. Found: C, 56.49; H, 4.53; N, 14.81.

2-Chloro-*N'*-(2-((4-oxo-3,4-dihydroquinazolin-2-yl)thio)acetyl)benzohydrazide (**17e**)

White solid; yield = 74%; mp 246–248 °C; $^1\text{H-NMR}$ (500 MHz; DMSO- d_6) δ_{H} 4.09 (s, 2H), 7.40–7.43 (m, 2H), 7.45–7.49 (m, 2H), 7.52 (d, $^3J = 7.5$ Hz, 1H), 7.59 (d, $^3J = 8.0$ Hz, 1H), 7.75 (t, $^3J = 7.5$ Hz, 1H), 8.02 (d, $^3J = 7.5$ Hz, 1H), 10.47 (s, 1H), 10.50 (br., 1H), 12.70 ppm (br., 1H); $^{13}\text{C-NMR}$ (125 MHz; DMSO- d_6) δ_{C} 32.04, 119.95, 125.74, 125.94, 126.21, 127.07, 129.28, 129.78, 130.39, 131.42, 134.54, 140.40, 148.25, 154.77, 161.14, 165.05, 166.22 ppm; Anal. Calcd for $\text{C}_{17}\text{H}_{13}\text{ClN}_4\text{O}_3\text{S}$: C, 52.51; H, 3.37; N, 14.41. Found: C, 52.21; H, 3.66; N, 14.74.

4-Chloro-*N'*-(2-((4-oxo-3,4-dihydroquinazolin-2-yl)thio)acetyl)benzohydrazide (**17f**)

White solid; yield = 86%; mp 257–259 °C; $^1\text{H-NMR}$ (500 MHz; DMSO- d_6) δ_{H} 4.11 (s, 2H), 7.42 (t, $^3J = 8.0$ Hz, 1H), 7.57 (d, $^3J = 8.5$ Hz, 2H), 7.60 (d, $^3J = 8.0$ Hz, 1H), 7.77 (t, $^3J = 8.5$ Hz, 1H), 7.87 (d, $^3J = 8.5$ Hz, 2H), 8.03 (d, $^3J = 7.5$ Hz, 1H), 10.39 (s, 1H), 10.60 (s, 1H), 12.70 ppm (br., 1H); $^{13}\text{C-NMR}$ (125 MHz; DMSO- d_6) δ_{C} 32.08, 119.94, 125.76, 125.97, 126.21, 128.57, 129.38, 131.08, 134.57, 136.70, 148.26, 154.75, 161.13, 164.37, 166.56 ppm; Anal. Calcd for $\text{C}_{17}\text{H}_{13}\text{ClN}_4\text{O}_3\text{S}$: C, 52.51; H, 3.37; N, 14.41. Found: C, 52.77; H, 3.05; N, 14.73.

2-Bromo-*N'*-(2-((4-oxo-3,4-dihydroquinazolin-2-yl)thio)acetyl)benzohydrazide (**17g**)

White solid; yield = 93%; mp 233–235 °C; $^1\text{H-NMR}$ (500 MHz; DMSO- d_6) δ_{H} 4.10 (s, 2H), 7.41–7.42 (m, 4H), 7.58 (t, $^3J = 8.0$ Hz, 1H), 7.66 (t, $^3J = 8.0$ Hz, 1H), 7.73–7.75 (m, 1H), 8.01 (t, $^3J = 8.0$ Hz, 1H), 10.46 (s, 1H), 10.50 (br., 1H), 12.69 ppm (br., 1H); $^{13}\text{C-NMR}$ (125 MHz; DMSO- d_6) δ_{C} 32.03, 119.27, 119.94, 125.73, 125.93, 126.20, 127.52, 129.30, 131.52, 132.91, 134.53, 136.56, 148.24, 154.78, 161.11, 165.85, 166.19 ppm; Anal. Calcd for $\text{C}_{17}\text{H}_{13}\text{BrN}_4\text{O}_3\text{S}$: C, 47.13; H, 3.02; N, 12.93. Found: C, 47.38; H, 3.32; N, 12.66.

N'-(2-((4-oxo-3,4,5,6,7,8-hexahydroquinazolin-2-yl)thio)acetyl)benzohydrazide (**18a**)

White powder; yield = 90%; mp 246–248 °C; $^1\text{H-NMR}$ (500 MHz; DMSO- d_6) δ_{H} 1.60–1.65 (m, 4H), 2.24–2.25 (m, 2H), 2.49 (ov., 2H), 3.96 (s, 2H), 7.44–7.47 (m, 2H), 7.54 (t, $^3J = 7.5$ Hz, 1H), 7.83 (d, $^3J = 7.5$ Hz, 2H), 10.23 (s, 1H), 10.44 (s, 1H), 12.52 ppm (br., 1H); $^{13}\text{C-NMR}$ (125 MHz; DMSO- d_6) δ_{C} 21.42, 21.77, 30.99, 31.92, 116.68, 127.43, 128.41, 131.81, 132.34, 156.28, 160.44, 162.73, 165.36, 166.66 ppm; Anal. Calcd for $\text{C}_{17}\text{H}_{18}\text{N}_4\text{O}_3\text{S}$: C, 56.97; H, 5.06; N, 15.63. Found: C, 56.67; H, 5.29; N, 15.92.

4-Methyl-*N'*-(2-((4-oxo-3,4,5,6,7,8-hexahydroquinazolin-2-yl)thio)acetyl)benzohydrazide (**18b**)

Off white powder; yield = 91%; mp 245–247 °C; $^1\text{H-NMR}$ (500 MHz; DMSO- d_6) δ_{H} 1.61–1.66 (m, 4H), 2.24–2.25 (br., 2H), 2.32 (s, 3H), 2.49 (br. ov, 2H), 3.95 (s, 2H), 7.26 (d, $^3J = 7.0$ Hz, 2H), 7.74 (d, $^3J = 6.5$ Hz, 2H), 10.19 (s, 1H), 10.35 (s, 1H), 12.52 ppm (br., 1H); $^{13}\text{C-NMR}$ (125 MHz; DMSO- d_6) δ_{C} 20.95, 21.41, 21.78, 30.96, 31.92, 116.84, 127.44, 128.91, 129.52, 141.79, 155.53, 160.59, 162.58, 165.21, 166.62 ppm; Anal. Calcd for $\text{C}_{18}\text{H}_{20}\text{N}_4\text{O}_3\text{S}$: C, 58.05; H, 5.41; N, 15.04. Found: C, 58.27; H, 5.23; N, 15.38.

4-Nitro-*N'*-(2-((4-oxo-3,4,5,6,7,8-hexahydroquinazolin-2-yl)thio)acetyl)benzohydrazide (**18c**)

Pale yellow powder; yield = 92%; mp 251–253 °C; $^1\text{H-NMR}$ (500 MHz; DMSO- d_6) δ_{H} 1.61–1.66 (m, 4H), 2.25 (br., 2H), 2.49 (br., 2H), 3.96 (s, 2H), 8.05 (d, $^3J = 8.5$ Hz, 2H), 8.31 (d, $^3J = 8.5$ Hz, 2H), 10.35 (s, 1H), 10.84 (br., 1H), 12.44 ppm (br., 1H); $^{13}\text{C-NMR}$ (125 MHz; DMSO- d_6) δ_{C} 21.43, 21.78, 30.98, 31.88, 116.60, 123.64, 129.01, 137.97, 149.38, 156.12, 161.02, 163.80, 166.59 ppm; Anal. Calcd for $\text{C}_{17}\text{H}_{17}\text{N}_5\text{O}_5\text{S}$: C, 50.61; H, 4.25; N, 17.36. Found: C, 50.89; H, 4.05; N, 17.63.

2-Methoxy-*N'*-(2-((4-oxo-3,4,5,6,7,8-hexahydroquinazolin-2-yl)thio)acetyl)benzohydrazide (**18d**)

Off white powder; yield = 93%; mp 212–214 °C; $^1\text{H-NMR}$ (500 MHz; DMSO- d_6) δ_{H} 1.60–1.66 (m, 4H), 2.25–2.26 (m, 2H), 2.49 (ov. br., 2H), 3.85 (s, 3H), 3.95 (s, 2H), 7.04 (t, $^3J = 7.5$ Hz, 1H), 7.14 (d, $^3J = 8.5$ Hz, 1H), 7.49 (t, $^3J = 7.0$ Hz, 1H), 7.69 (d, $^3J = 7.5$ Hz, 1H), 10.04 (s, 1H), 10.52 (br., 1H), 12.57 ppm (br., 1H); $^{13}\text{C-NMR}$

(125 MHz; DMSO- d_6) δ_C 21.41, 21.78, 30.97, 31.79, 55.95, 112.12, 116.53, 120.57, 121.12, 130.16, 130.41, 132.83, 157.01, 160.14, 162.47, 163.36, 165.59 ppm; Anal. Calcd for $C_{18}H_{20}N_4O_4S$: C, 55.66; H, 5.19; N, 14.42. Found: C, 55.45; H, 5.47; N, 14.08.

2-Chloro-*N'*-(2-((4-oxo-3,4,5,6,7,8-hexahydroquinazolin-2-yl)thio)acetyl)benzohydrazide (**18e**)

Off white powder; yield = 95%; mp 238-240 °C; 1H -NMR (500 MHz; DMSO- d_6) δ_H 1.61-1.65 (m, 4H), 2.26 (br. ov, 2H), 2.49 (br., 2H), 3.94 (s, 2H), 7.42-7.50 (m, 4H), 10.38 (s, 1H), 10.41 (s, 1H), 12.54 ppm (br., 1H); ^{13}C -NMR (125 MHz; DMSO- d_6) 21.40, 21.77, 30.92, 31.85, 116.59, 127.05, 127.99, 129.27, 129.77, 130.38, 131.41, 134.45, 160.36, 162.50, 165.01, 166.28 ppm; Anal. Calcd for $C_{17}H_{17}ClN_4O_3S$: C, 51.97; H, 4.36; N, 14.26. Found: C, 51.73; H, 4.62; N, 14.54.

4-Chloro-*N'*-(2-((4-oxo-3,4,5,6,7,8-hexahydroquinazolin-2-yl)thio)acetyl)benzohydrazide (**18f**)

white powder; yield = 95%; mp 252-254 °C; 1H -NMR (500 MHz; DMSO- d_6) δ_H 1.61-1.66 (m, 4H), 2.19-2.26 (br., 2H), 2.34-2.49 (m, 2H), 3.95 (s, 2H), 7.54 (d, $^3J = 8.0$ Hz, 2H), 7.85 (d, $^3J = 8.5$ Hz, 2H), 10.23 (s, 1H), 10.52 (s, 1H), 12.49 ppm (br., 1H); ^{13}C -NMR (125 MHz; DMSO- d_6) δ_C 21.40, 21.77, 30.95, 31.88, 116.34, 126.43, 128.54, 129.35, 131.06, 136.68, 160.13, 162.32, 164.31, 166.60 ppm; Anal. Calcd for $C_{17}H_{17}ClN_4O_3S$: C, 51.97; H, 4.36; N, 14.26. Found: C, 51.77; H, 4.72; N, 14.48.

2-Bromo-*N'*-(2-((4-oxo-3,4,5,6,7,8-hexahydroquinazolin-2-yl)thio)acetyl)benzohydrazide (**18g**)

White powder; yield = 94%; mp 248-250 °C; 1H -NMR (500 MHz; DMSO- d_6) δ_H 1.61-1.65 (m, 4H), 2.25-2.26 (m, 2H), 2.49 (br. ov, 2H), 3.94 (s, 2H), 7.38-7.45 (m, 3H), 7.65-7.67 (m, 1H), 10.39 (s, 2H), 12.55 ppm (br., 1H); ^{13}C -NMR (125 MHz; DMSO- d_6) δ_C 21.43, 21.80, 30.96, 31.88, 119.30, 127.57, 129.34, 131.58, 132.95, 132.96, 136.59, 156.27, 160.34, 162.55, 165.91, 166.35 ppm; Anal. Calcd for $C_{17}H_{17}BrN_4O_3S$: C, 46.69; H, 3.92; N, 12.81. Found: C, 46.45; H, 3.78; N, 12.57.

4.2. Biological evaluation

4.2.1. In vitro bioassay of cytotoxicity and antiviral activity

4.2.1.1. *MTT cytotoxicity assay.* The cytotoxic activity of the synthesized compounds were determined employing MTT assay as previously described [32]

4.2.1.2. *Inhibitory concentration 50 (IC₅₀) determination.* The values of IC₅₀ for the target quinazolines were determined as reported [34].

4.2.1.3. *Mechanism of action(s).* To investigate whether the most potent candidates affect the (a) viral adsorption, (b) viral replication, or (c) has a virucidal effect, the plaque infectivity reduction assay was performed according to the reported procedure [34].

4.3. Molecular modeling

Molecular docking studies were carried out using Molecular Operating Environment (MOE, 2020.0901) software. All minimizations were performed with MOE until an RMS gradient of 0.05 kcal•mol⁻¹•Å⁻² with MMFF94x force field and the partial charges were automatically calculated. The X-ray crystallographic structure of SARS-CoV-2 main protease (M^{PRO}) co-crystallized with a pyrimidine-2,4-dione inhibitor (YD1) (PDB ID: 7LTI) was downloaded from the protein data bank [36]. Water molecules and ligands which are not involved in the binding were first removed.

Next, the protein structure was prepared for the molecular docking study using *QuickPrep* protocol in MOE with the default options. YD1 exhibits several binding interactions with M^{PRO} active site with the amino acids Asn142, Gly143, Cys145, His163, Met165, Glu166, and Asp187 either directly or through water mediated interactions (Fig. 5). To perform the molecular docking study, the co-crystallized ligand (YD1) was used to define the active site and Triangle Matcher placement method and London dG scoring function were used.

The molecular docking protocol was first validated by self-docking of the co-crystallized ligand (YD1) in the vicinity of the enzyme active site. The self-docking step reproduced the co-crystallized ligand pose efficiently with docking score (S) of -13.26 kcal/mol and a root mean square deviation (RMSD) of 1.538 Å, moreover, the docking protocol reproduced all the key interactions with the active site amino acids indicating the suitability of the adopted molecular docking protocol for the intended molecular docking study (Fig. 6).

4.4. Estimation of physicochemical, pharmacokinetic and ADME properties

The open SwissADME web tool available from the Swiss Institute of Bioinformatics (SIB) was used for the calculation of the physicochemical descriptors as well as to predict the ADME parameters, and pharmacokinetic properties of the most potent compounds [37]. The compounds' structures were drawn on the web user interface, converted to SMILES notations, then submitted to the online server for calculation.

Author statement

Heba T. Abdel-Mohsen: Participated in the development of the idea of the project, organic synthesis of the target compounds, structure elucidation of the target compounds, analysis of the biological results, writing, revising and finalizing the manuscript.

Mohamed A. Omar: Participated in organic synthesis of the target compounds and revising the interpretation of NMR results.

Omnia Kutkat: Participated in analysis of the synthesized compounds for their antiviral activity.

Ahmed M. El Kerdawy: Run the computational studies to the target compounds, analysed the obtained results and revised the manuscript.

Alaa A. Osman: Participated in the in silico analyses of the target compounds.

Mohamed GabAllah: Participated in analysis of the synthesized compounds for their antiviral activity.

Ahmed Mostafa: Participated in the development of the idea of the project, analysis of the synthesized compounds for their antiviral activity and revising the biological part of the manuscript.

Mohamed A. Ali: Participated in the development of the idea of the project and revising the biological part of the manuscript.

Hoda I. El Diwani: Participated in the development of the idea of the project and revising the manuscript.

Declaration of Competing Interest

The authors have no conflict of interest to declare.

Data availability

Data will be made available on request.

Acknowledgments

Special thanks to National Research Centre (Egypt) for their fund through the project ID 12060119.

Supplementary materials

Supplementary material associated with this article can be found, in the online version, at doi:10.1016/j.molstruc.2022.134690.

References

- N. Chen, M. Zhou, X. Dong, J. Qu, F. Gong, Y. Han, Y. Qiu, J. Wang, Y. Liu, Y. Wei, J. Xia, T. Yu, X. Zhang, L. Zhang, Epidemiological and clinical characteristics of 99 cases of 2019 novel coronavirus pneumonia in Wuhan, China: a descriptive study, *Lancet* (London, England) 395 (10223) (2020) 507–513.
- T. Chen, D. Wu, H. Chen, W. Yan, D. Yang, G. Chen, K. Ma, D. Xu, H. Yu, H. Wang, T. Wang, W. Guo, J. Chen, C. Ding, X. Zhang, J. Huang, M. Han, S. Li, X. Luo, J. Zhao, Q. Ning, Clinical characteristics of 113 deceased patients with coronavirus disease 2019: retrospective study, *BMJ* 368 (2020) m1091.
- P. V'kovski, A. Kratzel, S. Steiner, H. Stalder, V. Thiel, Coronavirus biology and replication: implications for SARS-CoV-2, *Nat. Rev. Microbiol.* 19 (3) (2021) 155–170.
- H.A. Rothan, S.N. Byrareddy, The epidemiology and pathogenesis of coronavirus disease (COVID-19) outbreak, *J. Autoimmun.* 109 (2020) 102433.
- W.T. Harvey, A.M. Carabelli, B. Jackson, R.K. Gupta, E.C. Thomson, E.M. Harrison, C. Ludden, R. Reeve, A. Rambaut, C.-G.U. Consortium, S.J. Peacock, D.L. Robertson, SARS-CoV-2 variants, spike mutations and immune escape, *Nat. Rev. Microbiol.* 19 (7) (2021) 409–424.
- E.M. Saied, Y.A. El-Maradny, A.A. Osman, A.M.G. Darwish, H.H. Abo Nahas, G. Niedbala, M. Piekutowska, M.A. Abdel-Rahman, B.A. Balbool, A.M. Abdel-Azeem, A comprehensive review about the molecular structure of severe acute respiratory syndrome coronavirus 2 (SARS-CoV-2): insights into natural products against COVID-19, *Pharmaceutics* 13 (11) (2021).
- J. Zhao, S. Zhao, J. Ou, J. Zhang, W. Lan, W. Guan, X. Wu, Y. Yan, W. Zhao, J. Wu, J. Chodosh, Q. Zhang, COVID-19: coronavirus vaccine development updates, *Front. Immunol.* 11 (2020) 602256.
- A. Artese, V. Svicher, G. Costa, R. Salpini, V.C. Di Maio, M. Alkhatib, F.A. Ambrosio, M.M. Santoro, Y.G. Assaraf, S. Alcaro, F. Ceccherini-Silberstein, Current status of antivirals and druggable targets of SARS CoV-2 and other human pathogenic coronaviruses, *Drug Resist. Updat.* 53 (2020) 100721.
- A.C. Walls, Y.J. Park, M.A. Tortorici, A. Wall, A.T. McGuire, D. Veesler, Structure, function, and antigenicity of the SARS-CoV-2 spike glycoprotein, *Cell* 181 (2) (2020) 281–292 e6.
- A.A. Elifky, SARS-CoV-2 RNA dependent RNA polymerase (RdRp) targeting: an in silico perspective, *J. Biomol. Struct. Dyn.* 39 (9) (2021) 3204–3212.
- Z. Jin, X. Du, Y. Xu, Y. Deng, M. Liu, Y. Zhao, B. Zhang, X. Li, L. Zhang, C. Peng, Y. Duan, J. Yu, L. Wang, K. Yang, F. Liu, R. Jiang, X. Yang, T. You, X. Liu, X. Yang, F. Bai, H. Liu, X. Liu, L.W. Guddat, W. Xu, G. Xiao, C. Qin, Z. Shi, H. Jiang, Z. Rao, H. Yang, Structure of M(pro) from SARS-CoV-2 and discovery of its inhibitors, *Nature* 582 (7811) (2020) 289–293.
- J. Osipiuk, S.A. Azizi, S. Dvorkin, M. Endres, R. Jedrzejczak, K.A. Jones, S. Kang, R.S. Kathayat, Y. Kim, V.G. Lisnyak, S.L. Maki, V. Nicolaescu, C.A. Taylor, C. Tesar, Y.A. Zhang, Z. Zhou, G. Randall, K. Michalska, S.A. Snyder, B.C. Dickinson, A. Joachimiak, Structure of papain-like protease from SARS-CoV-2 and its complexes with non-covalent inhibitors, *Nat. Commun.* 12 (1) (2021) 743.
- S. Huff, I.R. Kummetha, S.K. Tiwari, M.B. Huante, A.E. Clark, S. Wang, W. Bray, D. Smith, A.F. Carlin, M. Endsley, T.M. Rana, Discovery and mechanism of SARS-CoV-2 main protease inhibitors, *J. Medicin. Chem.* (2021).
- R. Cannalire, C. Cerchia, A.R. Beccari, F.S. Di Leva, V. Summa, Targeting SARS-CoV-2 proteases and polymerase for COVID-19 treatment: state of the art and future opportunities, *J. Medicin. Chem.* (2020).
- R. Bansal, A. Malhotra, Therapeutic progression of quinazolines as targeted chemotherapeutic agents, *Eur. J. Med. Chem.* 211 (2021) 113016.
- R. Das, D.K. Mehta, M. Dhanawat, Bestowal of quinazoline scaffold in anticancer drug discovery, *Anticancer Agent. Med. Chem.* 21 (11) (2021) 1350–1368.
- D.S. Matharu, D.P. Flaherty, D.S. Simpson, C.E. Schroeder, D. Chung, D. Yan, J.W. Noah, C.B. Jonsson, E.L. White, J. Aube, R.K. Plemper, W.E. Severson, J.E. Golden, Optimization of potent and selective quinazolinones: inhibitors of respiratory syncytial virus that block RNA-dependent RNA-polymerase complex activity, *J. Medicin. Chem.* 57 (24) (2014) 10314–10328.
- G. Zhang, M. Wang, J. Zhao, Y. Wang, M. Zhu, J. Wang, S. Cen, Y. Wang, Design, synthesis and in vitro anti-influenza A virus evaluation of novel quinazoline derivatives containing S-acetamide and NH-acetamide moieties at C-4, *Eur. J. Med. Chem.* 206 (2020) 112706.
- J.R. Hwu, M. Kapoor, N.K. Gupta, S.C. Tsay, W.C. Huang, K.T. Tan, Y.C. Hu, P. Lysyen, J. Neyts, Synthesis and antiviral activities of quinazolinamine-coumarin conjugates toward chikungunya and hepatitis C viruses, *Eur. J. Med. Chem.* 232 (2022) 114164.
- J.Y. Lee, Y.S. Shin, J. Lee, S. Kwon, Y.H. Jin, M.S. Jang, S. Kim, J.H. Song, H.R. Kim, C.M. Park, Identification of 4-anilino-6-aminoquinazoline derivatives as potential MERS-CoV inhibitors, *Bioorg. Med. Chem. Lett.* 30 (20) (2020) 127472.
- J. Zhao, Y. Zhang, M. Wang, Q. Liu, X. Lei, M. Wu, S. Guo, D. Yi, Q. Li, L. Ma, Z. Liu, F. Guo, J. Wang, X. Li, Y. Wang, S. Cen, Quinoline and quinazoline derivatives inhibit viral RNA synthesis by SARS-CoV-2 RdRp, *ACS Infect. Dis.* 7 (6) (2021) 1535–1544.
- H.A. Rothan, T.C. Teoh, Cell-based high-throughput screening protocol for discovering antiviral inhibitors against SARS-CoV-2 main protease (3CLpro), *Mol. Biotechnol.* 63 (3) (2021) 240–248.
- G. Moyle, M. Boffito, A. Stoehr, A. Rieger, Z. Shen, K. Manhard, B. Sheedy, V. Hingorani, A. Raney, M. Nguyen, T. Nguyen, V. Ong, L.T. Yeh, B. Quart, Phase 2a randomized controlled trial of short-term activity, safety, and pharmacokinetics of a novel nonnucleoside reverse transcriptase inhibitor, RDEA806, in HIV-1-positive, antiretroviral-naïve subjects, *Antimicrob. Agents Chemother.* 54 (8) (2010) 3170–3178.
- P. Zhan, X. Li, Z. Li, X. Chen, Y. Tian, W. Chen, X. Liu, C. Pannecouque, E. De Clercq, Structure-based bioisosterism design, synthesis and biological evaluation of novel 1,2,4-triazin-6-ylthioacetamides as potent HIV-1 NNRTIs, *Bioorg. Med. Chem. Lett.* 22 (23) (2012) 7155–7162.
- G.N. Zhang, Q. Li, J. Zhao, X. Zhang, Z. Xu, Y. Wang, Y. Fu, Q. Shan, Y. Zheng, J. Wang, M. Zhu, Z. Li, S. Cen, J. He, Y. Wang, Design and synthesis of 2-((1H-indol-3-yl)thio)-N-phenyl-acetamides as novel dual inhibitors of respiratory syncytial virus and influenza virus A, *Eur. J. Med. Chem.* 186 (2020) 111861.
- M. Yu, A. Liu, G. Du, L. Naesens, E. Vanderlinden, E. De Clercq, X. Liu, Discovery of dihydro-alkoxy-benzyl-oxopyrimidines as promising anti-influenza virus agents, *Chem. Biol. Drug Des.* 78 (4) (2011) 596–602.
- P. Zhan, L. Wang, H. Liu, X. Chen, X. Li, X. Jiang, Q. Zhang, X. Liu, C. Pannecouque, L. Naesens, E. De Clercq, A. Liu, G. Du, Arylazolyl(aziny)thioacetanilide. Part 9: Synthesis and biological investigation of thiazolylthioacetamides derivatives as a novel class of potential antiviral agents, *Arch. Pharm. Res.* 35 (6) (2012) 975–986.
- S.-Y. Chou, W.-K. Yin, Y.-S. Chung, L.-S. Chang, C.-W. Liu, S.-F. Chen, K.-S. Shih, Kilogram-scale synthesis of a highly selective α_1 -adrenoceptor antagonist (DL-028A), *Org. Process Res. Dev.* 6 (3) (2002) 273–278.
- H.T. Abdel-Mohsen, M.A. Omar, A. Petreni, C.T. Supuran, Novel 2-substituted thioquinazoline-benzenesulfonamide derivatives as carbonic anhydrase inhibitors with potential anticancer activity, *Arch. Pharm. (Weinheim)* (2022) e2200180.
- H.T. Abdel-Mohsen, J. Conrad, K. Harms, D. Nohr, U. Beifuss, Laccase-catalyzed green synthesis and cytotoxic activity of novel pyrimidobenzothiazoles and catechol thioethers, *RSC Adv.* 7 (28) (2017) 17427–17441.
- H.T. Abdel-Mohsen, A. Petreni, C.T. Supuran, Investigation of the carbonic anhydrase inhibitory activity of benzenesulfonamides incorporating substituted fused-pyrimidine tails, *Arch. Pharm. (Weinheim)* 355 (11) (2022) e2200274.
- T. Mosmann, Rapid colorimetric assay for cellular growth and survival: application to proliferation and cytotoxicity assays, *J. Immunol. Methods.* 65 (1) (1983) 55–63.
- A. Kandeil, A. Mostafa, R. El-Shesheny, M. Shehata, W.H. Roshdy, S.S. Ahmed, M. Gomaa, A.E. Taweel, A.E. Kayed, S.H. Mahmoud, Y. Moatasim, O. Kutkat, M.N. Kamel, M. Mahrous, M.E. Sayes, N.M.E. Guindy, A. Naguib, M.A. Ali, Coding-complete genome sequences of two SARS-CoV-2 isolates from Egypt, *Microbiol. Resour. Anounc.* 9 (22) (2020).
- A. Mostafa, A. Kandeil, A.M.M.E. Y, O. Kutkat, Y. Moatasim, A.A. Rashad, M. Shehata, M.R. Gomaa, N. Mahrous, S.H. Mahmoud, M. GabAllah, H. Abbas, A.E. Taweel, A.E. Kayed, M.N. Kamel, M.E. Sayes, D.B. Mahmoud, R. El-Shesheny, G. Kayali, M.A. Ali, FDA-approved drugs with potent in vitro antiviral activity against severe acute respiratory syndrome Coronavirus 2, *Pharmaceutics* (Basel) 13 (12) (2020).
- H.M. Mengist, T. Dilnessa, T. Jin, Structural Basis of Potential Inhibitors Targeting SARS-CoV-2 Main Protease, *Front Chem* 9 (2021) 622898.
- A. Clyde, S. Galanie, D.W. Kneller, H. Ma, Y. Babuji, B. Blaiszik, A. Brace, T. Brettin, K. Chard, R. Chard, L. Coates, I. Foster, D. Hauner, V. Kertes, N. Kumar, H. Lee, Z. Li, A. Merzky, J.G. Schmidt, L. Tan, M. Titov, A. Trifan, M. Turilli, H. Van Dam, S.C. Chennubhotla, S. Jha, A. Kovalevsky, A. Ramanathan, M.S. Head, R. Stevens, High-throughput virtual screening and validation of a SARS-CoV-2 main protease noncovalent inhibitor, *J. Chem. Inform. Model.* 62 (1) (2022) 116–128.
- A. Daina, O. Michielin, V. Zoete, SwissADME: a free web tool to evaluate pharmacokinetics, drug-likeness and medicinal chemistry friendliness of small molecules, *Sci. Rep.* 7 (2017) 42717.
- A. Daina, O. Michielin, V. Zoete, iLOGP: a simple, robust, and efficient description of n-octanol/water partition coefficient for drug design using the GB/SA approach, *J. Chem. Inform. Model.* 54 (12) (2014) 3284–3301.
- M.L. Amin, P-glycoprotein inhibition for optimal drug delivery, *Drug Target Insight.* 7 (2013) 27–34.
- C.A. Lipinski, F. Lombardo, B.W. Dominy, P.J. Feeney, Experimental and computational approaches to estimate solubility and permeability in drug discovery and development settings, *Adv. Drug. Deliv. Rev.* 46 (1–3) (2001) 3–26.
- D.F. Veber, S.R. Johnson, H.Y. Cheng, B.R. Smith, K.W. Ward, K.D. Kopple, Molecular properties that influence the oral bioavailability of drug candidates, *J. Medicin. Chem.* 45 (12) (2002) 2615–2623.
- A.K. Ghose, V.N. Viswanadhan, J.J. Wendoloski, A knowledge-based approach in designing combinatorial or medicinal chemistry libraries for drug discovery. I. A qualitative and quantitative characterization of known drug databases, *J. Comb. Chem.* 1 (1) (1999) 55–68.
- W.J. Egan, K.M. Merz Jr., J.J. Baldwin, Prediction of drug absorption using multivariate statistics, *J. Medicin. Chem.* 43 (21) (2000) 3867–3877.
- I. Muegge, S.L. Heald, D. Brittelli, Simple selection criteria for drug-like chemical matter, *J. Medicin. Chem.* 44 (12) (2001) 1841–1846.
- J.B. Baell, G.A. Holloway, New substructure filters for removal of pan assay interference compounds (PAINS) from screening libraries and for their exclusion in bioassays, *J. Medicin. Chem.* 53 (7) (2010) 2719–2740.